Conventional and Non-conventional Global Alfvén Eigenmodes (GAE and NGAE) in stellarators

Ya. I. Kolesnichenko, V. V. Lutsenko

Institute for Nuclear Research, Prospekt Nauky 47, Kyiv 03680, Ukraine

A. Weller, A. Werner

Max-Planck-Institut für Plasmaphysik,

*IPP-EURATOM Association, D-17491 Greifswald, Germany**

Yu. V. Yakovenko

Institute for Nuclear Research, Prospekt Nauky 47, Kyiv 03680, Ukraine

J. Geiger

Max-Planck-Institut für Plasmaphysik,

IPP-EURATOM Association, D-17491 Greifswald, Germany

O. P. Fesenyuk

Institute for Nuclear Research, Prospekt Nauky 47, Kyiv 03680, Ukraine

(Dated: August 31, 2007)

Conditions of the existence of the Global Alfvén Eigenmodes (GAE) and Non-conventional Global Alfvén Eigenmodes (NGAE) predicted for stellarators by Ya. I. Kolesnichenko *et al.* [Phys. Rev. Lett. **94**, 165004 (2005)] have been obtained. It is found that they depend on the nature of the rotational transform and that conditions for NGAE can be most easily satisfied in currentless stellarators. It is shown that the plasma compressibility may play an important role for the modes with the frequency about or less than that of the Toroidicity-induced Alfvén Eigenmodes (TAE). It is found that features of the Alfvén continuum in the vicinity of the $k_{\|} = 0$ radius ($k_{\|}$ is the longitudinal wave number) can be very different, depending on a parameter which we refer to as "the sound parameter". Specific calculations modeling low-frequency Alfvén instabilities in the stellarator Wendelstein 7-AS [A. Weller *et al.*, Phys. Plasmas **8**, 931 (2001)] are carried out, which are in reasonable agreement

with the observations. It is emphasized that experimental data on low-frequency Alfvénic activity can be used for the reconstruction of the profile of the rotational transform. The mentioned results are obtained with the use of the equations derived in this paper for the GAE/NGAE modes and of the codes COBRAS and BOA-fe.

PACS numbers: 52.35.Bj; 52.55.Hc; 52.65.Kj

Keywords: stellarator; Alfvén continuum; Alfvén eigenmodes

I. INTRODUCTION

Alfvén instabilities driven by energetic ions were observed in many experiments on tokamaks, stellarators, and spherical tori.[1–3] These instabilities can have very different forms and consequences. They are not necessarily harmful and can be used for diagnostics.[4] There is an idea to destabilize Alfvén eigenmodes by external antennas in a reactor for ash removal.[5]

In stellarators, Alfvén instabilities have a number of peculiarities. In particular, there are more various kinds of eigenmodes in stellarators than in tokamaks [namely, there are Mirror-induced Alfvén Eigenmodes (MAE) and various Helicity-induced Alfvén Eigenmodes (HAE) in the high frequency part of the Alfvén spectrum[6–8]]; there exist also non-axisymmetric resonances of the wave-particle interaction and resonances associated with the finite orbit width of the energetic ions;[5,9] the high-frequency modes are strongly localized poloidally (typically having anti-ballooning structure);[10] thermal crashes may occur during Alfvén instabilities.[2]

Many features of Alfvén instabilities are associated with the features of the Alfvén continuum. In the upper part of the Alfvén spectrum, continuum regions are compressed into extremely narrow threads, so that the gaps in the continuum strongly dominate. Instabilities in this part of the spectrum represent destabilized gap modes and EPMs (Energetic Particle Modes) associated with the lack of the axial symmetry in stellarators. In contrast to this, in the lower part of the Alfvén spectrum, continuum regions dominate, whereas the gaps in the continuum are narrow. Therefore, the low frequency instabilities represent either destabilized gap modes or continuum modes. They occur in all toroidal plasma systems. In

*Electronic address: arthur.weller@ipp.mpg.de

stellarators, low frequency instabilities are typically present in all experiments with Alfvénic activity induced by fast ions.

In this paper, we study low frequency instabilities associated with the destabilization of modes in the continuous part of the spectrum. A well-known mode of this kind is the Global Alfvén Eigenmode (GAE).[11] The GAE is a mode with the frequency below a minimum of a continuum branch with given mode numbers (m and n). Another mode is the Non-conventional Global Alfvén Eigenmode (NGAE), which is a mode with the frequency above a maximum of a continuum branch with given mode numbers. The NGAE was found in a currentless stellarator plasma with a slightly non-monotonic rotational transform; furthermore, it was argued that the NGAE can generate a Kinetic Alfvén Wave (KAW) leading to anomalous electron heat transfer and sheared plasma rotation.[9,12] In fact, this raised several fundamental questions, which are of interest not only for stellarator plasmas, but also for any plasma, in particular, for reversed-shear plasmas of tokamaks. Note that a similar mode, the Alfvén Cascade Mode (ACM) or Reversed Shear Alfvén Eigenmode (RSAE), was found in the tokamak JET (Joint European Torus).[13] However, ACMs occur during so called "Alfvén cascades" where instabilities with various mode numbers arise successively, which was not observed in stellarators. The temporal evolution of the ACM frequency is completely different from the NGAE frequency evolution observed in the stellarator Wendelstein 7-AS (W7-AS).[2] In addition, ACMs are localized near the radius where the tokamak safety factor is minimum (i.e., where the rotational transform has a maximum), whereas the maximum of the NGAE mode can be located far from this point in small-shear devices.

The GAE/NGAE frequency can be either below the toroidicity-induced gap in the Alfvén continuum or above it. But it is known that when the mode frequency is much less than the frequency of the Toroidicity-induced Alfvén Eigenmodes (TAE), the Alfvén spectrum in tokamaks can be strongly affected by the plasma compressibility.[15] One can expect that this will be the case in stellarators, too. In addition, probably effects of the compressibility can be considerable also for TAEs and for NGAEs with the frequencies slightly above the TAE gap. Effects of the compressibility on Alfvén modes in stellarators are studied in this paper.

This work was stimulated by observations of low-frequency Alfvénic activity in Wendelstein 7-AS.[2] A W7-AS discharge where various quasi-steady state low frequency Alfvén instabilities occurred simultaneously was selected for analysis, and a numerical simulation of the destabilized modes was carried out, using equations derived in this work.

The structure of the work is as follows. In Sec. II the equations describing GAE/NGAE modes in incompressible plasmas are derived and analyzed. Effects of the plasma compressibility are studied in Sec. III on the basis of equations derived in this section. Section IV deals with modeling of instabilities in a W7-AS discharge. The obtained results are summarized in Sec. V.

II. GAE AND NGAE MODES IN COLD INCOMPRESSIBLE PLASMAS

We employ a perturbative approach, assuming that the fast ions weakly affect the Alfvén eigenmodes, whose existence and spatial structure are determined by the bulk plasma. We make an assumption (usual for the ideal magnetohydrodynamics) that $\widetilde{E}_\parallel = 0$, where $\widetilde{E}_\parallel$ is the perturbed electric field along the equilibrium magnetic field, $\mathbf{B}_0$, tilde labels perturbed quantities. In addition, we assume that $\widetilde{B}_\parallel = 0$ ($\widetilde{B}_\parallel$ is the perturbed longitudinal magnetic field) in order to exclude from the consideration fast magnetoacoustic waves. Due to these assumptions, we can take $\widetilde{\mathbf{A}}_\perp = 0$ ($\widetilde{\mathbf{A}}_\perp$ is the transverse component of the perturbed vector potential) and describe Alfvén eigenmodes by a single equation for the scalar potential of the electromagnetic field ($\widetilde{\Phi}$), at least, when effects of the plasma compressibility and finite pressure are not important. The scalar potential $\widetilde{\Phi}$ is connected with the electromagnetic field strength by the equations:

$$\widetilde{\mathbf{E}} = -\nabla_\perp \widetilde{\Phi}, \quad \widetilde{\mathbf{B}} = \nabla \times \widetilde{A}\mathbf{b}, \quad \widetilde{A} = \frac{ck_\parallel}{\omega}\widetilde{\Phi}, \tag{1}$$

where $\widetilde{A} \equiv \widetilde{A}_\parallel$ is the longitudinal component of the scalar potential of the electromagnetic field, $\nabla_\perp = \nabla - \mathbf{b}\cdot\nabla$, $\mathbf{b} = \mathbf{B}_0/B_0$, ω is the mode frequency, $k_\parallel$ is the longitudinal wave number. We choose perturbations in the form

$$\widetilde{\Phi} = \sum_{mn} \Phi_{mn}(\psi)\exp(-i\omega t - in\varphi + im\vartheta), \tag{2}$$

where ψ, ϑ, and φ are Boozer coordinates. Then $k_\parallel = (m\iota - n)/R$, where ι is the rotational transform, m and n are the poloidal mode number and toroidal mode number, respectively, R is the major radius of the torus. Following the procedure of Ref. 6 and neglecting the coupling between Fourier harmonics of $\widetilde{\Phi}$, we obtain the following equation describing Alfvén eigenmodes:

$$\frac{1}{r}\frac{\partial}{\partial r} r\left(k_\parallel^2 - \frac{\omega^2}{v_A^2}\right)\frac{\partial \Phi_{mn}}{\partial r} - \left[\frac{m^2}{r^2}\left(k_\parallel^2 - \frac{\omega^2}{v_A^2}\right) - \frac{k_\parallel}{r}(rk_\parallel')'\right]\Phi_{mn} + \frac{4\pi i\omega}{c^2}\mathbf{B}_{mn}\cdot\nabla_\perp\frac{j_{0\parallel}}{B_0} = 0, \tag{3}$$

where the radial coordinate r is defined by $\psi = \bar{B}r^2/2$, with $\bar{B}$ the average equilibrium magnetic field at the magnetic axis, $j_{0\parallel}$ is the unperturbed plasma current density, prime here and below denotes the radial derivative (d/dr).

Sometimes it is convenient to use another wave function, $\Psi = \widetilde{\Phi}/r$, instead of $\widetilde{\Phi}$. This function, as one can show, is proportional to the poloidal component of the electric field, $\widetilde{E}_{\rm pol}$, and $\widetilde{E}_{\rm pol}$ is proportional to the plasma radial displacement, ξ_r. Proceeding to this variable, we write Eq. (3) as follows:

$$\frac{1}{r}\frac{\partial}{\partial r}r^3\left(k_\parallel^2-\frac{\omega^2}{v_A^2}\right)\frac{\partial\Psi_{mn}}{\partial r}-(m^2-1)\left(k_\parallel^2-\frac{\omega^2}{v_A^2}\right)\Psi_{mn}-\omega^2\left(\frac{1}{v_A^2}\right)'r\Psi_{mn}$$
$$+rk_\parallel(3k_\parallel'+rk_\parallel'')\Psi_{mn}+\frac{4\pi i\omega}{c^2}r\mathbf{B}_{mn}\cdot\nabla_\perp\frac{j_{0\parallel}}{B_0}=0. \qquad (4)$$

The plasma current $j_{0\parallel}$ contributes to the production of the rotational transform in stellarators and is completely responsible for the rotational transform in tokamaks. It is determined by the radial derivative of a covariant component of the magnetic field, B_ϑ, as follows:

$$j_{0\parallel}\approx\frac{c}{4\pi}\frac{1}{r}\frac{\partial}{\partial r}B_\vartheta. \qquad (5)$$

In order to express B_ϑ through the rotational transform, we note that

$$\iota=\frac{B^\vartheta}{B^\varphi}=\frac{g^{\vartheta\vartheta}B_\vartheta}{B^\varphi}+\frac{g^{\vartheta\varphi}B_\varphi}{B^\varphi}, \qquad (6)$$

where the subscripts/superscripts denote co/contra-variant vector components, g^{ij} are contravariant metric tensor components. The first term in the RHS of Eq. (6) represents the partial rotational transform associated with the plasma current (B_ϑ in Boozer coordinates is actually the toroidal plasma current), whereas the second term, which we denote as $\iota_{\rm ext}$, is the partial rotational transform associated with the external coils. Of course, these statements are exact only in the limit cases when either the plasma current is completely responsible for the rotational transform (tokamak case) or this current is absent because, strictly speaking, the equilibrium and, thus, the metric tensor components depend on the presence of the plasma current. We obtain from Eq. (6) that $B_\vartheta=(\iota-\iota_{\rm ext})B^\varphi/g^{\vartheta\vartheta}$. This leads to

$$j_{0\parallel}\approx\frac{c\bar{B}}{4\pi rR}\frac{\partial}{\partial r}r^2\iota\nu_\iota, \qquad (7)$$

where $\nu_\iota=(\iota-\iota_{\rm ext})/\iota$ is the fraction of the rotational transform associated with the plasma current. It is clear that in tokamaks $\nu_\iota=1$, whereas in stellarators ν_ι can be negligibly small.

Using Eqs. (7) and (1), we can write the current term in Eq. (4) as

$$C_{mn}^{(j)} \equiv \frac{4\pi i\omega}{c^2}\mathbf{B}_{mn}\cdot\nabla_\perp\frac{j_{0\parallel}}{B_0} = -k_\parallel\frac{m}{R}\left[(3\iota' + r\iota'')\nu_\iota + (2r\iota' + 3\iota)\frac{d\nu_\iota}{dr} + r\iota\frac{d^2\nu_\iota}{dr^2}\right]\Psi_{mn}. \qquad (8)$$

It follows from Eq. (8) that the current term completely compensates the shear terms in Eq. (4) when $\nu_\iota = 1$ (the tokamak case). This implies that conditions of existence of Alfvén eigenmodes that are sensitive to the magnetic shear are different in stellarators and tokamaks.

To find these conditions, we reduce Eq. (4) to a Schrödinger-like equation. This can be done by proceeding to a new wave function, $Y = \Psi_{mn}r^{3/2}\left(k_\parallel^2 - \omega^2/v_A^2\right)^{0.5}$. This change of variables eliminates the terms proportional to the first derivative of the wave function, leading to the following equation:

$$\frac{d^2Y}{dr^2} - G(r)Y = 0, \qquad (9)$$

where

$$\begin{aligned} G(r) \;=\; & \frac{m^2 - 1/4}{r^2} - \frac{1}{4}\left(\frac{P'}{P}\right)^2 + \frac{3}{2r}\frac{P'}{P} + \frac{P''}{2P} \\ & + \frac{1}{rP}\left[\frac{\omega^2}{v_A^2}\frac{\rho'}{\rho} - k_\parallel\left(3k_\parallel' + rk_\parallel''\right)(1-\nu_\iota) + k_\parallel\left(2rk_\parallel' + \frac{3m\iota}{R}\right)\frac{d\nu_\iota}{dr} + \iota k_\parallel r\frac{m}{R}\frac{d^2\nu_\iota}{dr^2}\right], \qquad (10) \end{aligned}$$

$P = k_\parallel^2 - \omega^2/v_A^2$, and ρ is the mass density. This equations can be considered as a Schrödinger equation with the full energy equal to zero. Then a condition of the existence of solutions can be written as $G = 0$ in a pair of points, which correspond to "turning points". A more general condition is

$$G < 0 \qquad (11)$$

in some region. Equation (11) provides the existence of solutions even when $G < 0$ everywhere in the plasma ($0 \le r \le a$) provided that $Y(a) = 0$. The mentioned boundary condition implies that we have to set the "potential energy" G to infinity for $r \ge a$, thus providing the presence of turning points. It is clear that when the points where $G = 0$ exist and are not close to the plasma boundary, the solution is weakly dependent on the boundary conditions.

The equation for Alfvén eigenmodes can be written in a form of the Schrödinger equation with the potential energy convenient for analytical consideration when the mode is well

localized. We assume that a mode is localized around the radius r_* where the Alfvén continuum, $\omega_A(r)$, has an extremum. In the considered approximation, the Alfvén continuum is determined by the equation $\omega_A^2 = k_\parallel^2(r)v_A^2(r)$, which leads to r_* determined by the equation

$$k_\parallel R = 2m\iota' \frac{\rho}{\rho'}. \tag{12}$$

Following the approach of Ref. 16, we approximate $\omega_A^2(r)$ as

$$\omega_A^2(r) = \omega_{A*}^2 + 0.5(\omega_A^2)''_*(r - r_*)^2, \tag{13}$$

with $\omega_{A*} = \omega_A(r_*)$, $(\omega_A^2)'' \equiv d^2\omega_A^2/dr^2$ and proceed to the variable

$$x = \frac{r - r_*}{\Delta}, \tag{14}$$

where $\Delta^2 = 2(\omega_{A*}^2 - \omega^2)/(\omega_A^2)''_*$. Then, taking into account that

$$\frac{P'}{P} \approx \left.\frac{\rho'}{\rho}\right|_{r*} + \frac{2x}{\Delta(1+x^2)} \tag{15}$$

for $(\omega^2 - \omega_{A*}^2) \ll \omega_{A*}^2$, we obtain the following Schrödinger equation for well-localized modes:

$$\frac{d^2Y}{dx^2} + [\mathcal{E} - U(x)]Y = 0. \tag{16}$$

Here $\mathcal{E} \equiv -(m^2 - 1/4)\Delta^2/r_*^2$ plays the role of the full energy and $U(x)$ the potential energy,

$$U(x) = \frac{1}{(1+x^2)^2} - \frac{g}{1+x^2}, \tag{17}$$

with g a parameter given by

$$g = g^T \frac{1}{2}\left[3\nu_\iota - 1 - (1-\nu_\iota)\frac{\iota'' r}{\iota'} + \left(2r + \frac{3\iota}{\iota'}\right)\frac{d\nu_\iota}{dr} + \frac{r\iota}{\iota'}\frac{d^2\nu_\iota}{dr^2}\right]_{r_*}, \tag{18}$$

$g^T \equiv g(\nu_\iota = 1)$, i.e., g^T is g in tokamaks,

$$g^T = -\frac{2\omega_{A*}^2}{r_*(\omega_A^2)''_*}\frac{\rho'}{\rho} = \frac{2}{r_*}\left(\frac{\rho''}{\rho'} - \frac{\rho'}{2\rho} - \frac{\iota''}{\iota'}\right)^{-1}\Bigg|_{r_*}. \tag{19}$$

The potential energy has a minimum at $x = 0$ when $g > 2$ and a pair of minima located at $x_{\min} = \pm\sqrt{2/g - 1}$ and separated by a maximum at $x = 0$ when $0 < g < 2$, as shown in Fig. 1. The function $U(x)$ is negative in the points of minima, which means that eigensolutions of Eq. (16) with discrete energy eigenvalues exist in the region of $\mathcal{E} < 0$,

i.e., for $\Delta^2 > 0$. This corresponds to eigenfrequencies below the Alfvén continuum for $(\omega_A^2)'' > 0$ and above the continuum for $(\omega_A^2)'' < 0$:

$$\omega^2 = \omega_{A*}^2 \left[1 + \frac{r_*^2 (\omega_{A*}^2)''}{2(m^2 - 1/4)\omega_{A*}^2} \, \mathcal{E} \right]. \tag{20}$$

When $g \ll 1$, the potential well becomes very shallow, and $x_{\min} \gg 1$. To consider this case, it is more convenient to use new variables defined by $x = \sinh \zeta$, $Y = \sqrt{\cosh \zeta}\, Z(\zeta)$. Then Eq. (16) takes the form:

$$\frac{d^2 Z}{d\zeta^2} + [\mathcal{E}_1 - V(\zeta)]\, Z = 0, \tag{21}$$

where

$$\mathcal{E}_1 = g - \frac{1}{4}, \quad V(\zeta) = \frac{1}{4 \cosh^2 \zeta} + \frac{(m^2 - 1/4)\Delta^2}{r_*^2} \cosh^2 \zeta. \tag{22}$$

It follows from Eq. (21) that solutions exist only when

$$g > 1/4, \tag{23}$$

where g is given by Eqs. (18) and (19). Note that this condition, as well as solutions of Eq. (21) with $\mathcal{E}_1$ and V given by Eq. (22), were obtained for a second-order differential equation equivalent to Eq. (16) in Ref. 17.

Let us consider specific examples relevant to tokamaks ($\nu_\iota = 1$) and currentless stellarators ($\nu_\iota = 0$). Then Eq. (18) is reduced to

$$g^S = -\frac{1}{2} \left(1 + \frac{\iota'' r}{\iota'} \right) \Bigg|_{r*} g^T, \tag{24}$$

where the superscript S means that the magnitude is relevant to currentless stellarators.

We assume first that the iota profile is monotonic and take it in the form:

$$\iota = \iota_0 \left(1 + \alpha \frac{r^2}{a^2} \right)^\sigma, \tag{25}$$

where a is the plasma radius, α is a parameter, $\alpha > -1$. Then we obtain from Eq. (24):

$$g^S = -\frac{1 + \alpha\sigma r_*^2/a^2}{1 + \alpha r_*^2/a^2} \, g^T. \tag{26}$$

It follows from Eq. (26) that the signs of g^S and g^T are always different for $\alpha\sigma > 0$, i.e., when $\iota(r)$ is a growing function. These signs coincide only when the following two conditions are satisfied simultaneously: $\alpha\sigma < 0$ and $|\alpha\sigma| r_*^2/a^2 > 1$, i.e., when $\iota(r)$ is a decreasing function

and the magnetic shear is very large. In particular, $g^S = -g^T$ for $\sigma = 1$. The same equation approximately holds also for any small magnetic shear ($|\alpha| \ll 1$, $|\sigma| \ll 1$). Thus, when $\iota(r)$ is a monotonic function given by Eq. (25), GAE modes in stellarators exist only for those plasma parameters for which GAEs are absent in tokamaks, except for a large-shear case with $\iota' < 0$.

In order to evaluate g^T, we specify $\rho(r)$ as

$$\rho(r) = \rho_0(1 - \gamma r^2/a^2)^\delta, \tag{27}$$

where $\delta > 0$ and $0 < \gamma < 1$ are parameters. Then

$$g^T = \frac{2a^2}{r_*^2}\left[\frac{(2-\delta)\gamma}{1-\gamma r^2/a^2} + \frac{2\alpha(1-\sigma)}{1+\alpha r^2/a^2}\right]^{-1}_{r*}. \tag{28}$$

It follows from Eq. (28) that the parameters $\delta < 2$, $\sigma \leq 1$, $\alpha > 0$ lead to $g^T > 0$. On the other hand, the parameters $\delta > 2$, $\sigma > 1$, $\alpha > 0$ lead to $g^T < 0$; the same sign of g^T takes place when $\sigma < 1$, $\alpha < 0$, $|\alpha| r^2/a^2 < 1$. In a particular low-shear case with $\sigma \ll 1$ and a steep density gradient, $\delta = 2$, we have

$$g^S = -\frac{g^T}{1+\alpha r_*^2/a^2} = -\frac{a^2}{r_*^2\alpha}. \tag{29}$$

Now we proceed to the case of non-monotonic $\iota(r)$. Let us assume that r_* is localized close to the point r_m where $\iota(r)$ has an extremum, which implies due to Eq. (12) that either the plasma is homogeneous in the region of the mode localization and/or the mode frequency lies well below the TAE-gap in Alfvén continuum ($k_\| R \ll \iota$). Then we conclude from Eqs. (19) and (24) that $g^S \to 1$, whereas $g^T \to 0$. This means that the condition given by Eq. (23) is well satisfied in stellarators and, thus, eigenmodes exist; depending on the sign of $(\omega_A^2)''$, they can be either GAEs (when ω_A has a minimum) or NGAEs (when ω_A has a maximum). In addition, the obtained result ($g^T = 0$) explains why taking into account additional factors (such as the presence of the energetic ions,[18] the toroidicity,[19] and the plasma density gradient[20]) is necessary to calculate RSAE modes in tokamaks.

III. EFFECTS OF COMPRESSIBILITY

Although in many cases Alfvén waves are studied in the approximation of incompressible plasma, features of these waves and even conditions of their existence may depend on the

plasma compressibility. Effects of the compressibility on Alfvén waves will be studied in this section.

We proceed from the following equation, which generalizes Eq. (3) by taking into account the compressibility, $\widetilde{\zeta}$ ($\widetilde{\zeta} \equiv \mathrm{div}\,\boldsymbol{\xi}$, with $\boldsymbol{\xi}$ the plasma displacement) and the coupling between Fourier harmonics of Φ_{mn} (we used Ref. 21):

$$\omega^2 \nabla \cdot \left(\frac{1}{v_A^2 h_B^2} \nabla_\perp \widetilde{\Phi} \right) + B_0 \nabla_\parallel \left\{ \frac{1}{B_0^2} \nabla \cdot \left[B_0^2 \nabla_\perp \left(\frac{1}{B_0} \nabla_\parallel \widetilde{\Phi} \right) \right] \right\} - C^{(j)} + C^{(s)} = 0, \qquad (30)$$

where $\nabla_\parallel = \mathbf{b} \cdot \nabla$, $\nabla_\perp = \nabla - \mathbf{b} \nabla_\parallel$, $C^{(j)}$ is the current term with Fourier harmonics given by Eq. (8), $C^{(s)}$ is the term associated with the plasma compressibility,

$$C^{(s)} = \frac{2i\omega}{c} \nabla \cdot \left(\beta_s h_B^{-2} \mathbf{B}_0 \times \boldsymbol{\mathcal{K}} \widetilde{\zeta} \right), \qquad (31)$$

$\beta_s = c_s^2 / v_A^2$, $c_s = (\gamma p / \sum_i M_i n_i)^{0.5}$ is the sound velocity, M_i and n_i are the ion mass and density, respectively, p is the plasma pressure, $\boldsymbol{\mathcal{K}} = (\mathbf{b} \cdot \nabla)\mathbf{b}$ is the field line curvature.

In low-β plasmas the compressibility is connected to the scalar potential of the electric field as follows:[21]

$$\left[\omega^2 + c_s^2 B_0 \nabla_\parallel \left(\frac{1}{B_0} \nabla_\parallel \right) \right] \widetilde{\zeta} = \frac{2ic\omega}{B_0^2} (\mathbf{B}_0 \times \boldsymbol{\mathcal{K}}) \cdot \nabla \widetilde{\Phi}. \qquad (32)$$

Equations (30) and (32) for $\widetilde{\Phi}$ and $\widetilde{\zeta}$ describe ideal-MHD (magnetohydrodynamics) Alfvén waves and sound waves coupled due to the field line curvature. To study Alfvén waves, it is convenient to eliminate $\widetilde{\zeta}$. This will be done below.

Let us write Fourier series for the curvature and the magnetic field:

$$\boldsymbol{\mathcal{K}} = \sum_{\mu\nu} \boldsymbol{\mathcal{K}}^{(\mu\nu)} e^{i\mu\vartheta - i\nu N\varphi}, \quad B_0 = \bar{B} \left(1 + \frac{1}{2} \sum_{\mu\nu} \epsilon_B^{(\mu\nu)} e^{i\mu\vartheta - i\nu N\varphi} \right), \qquad (33)$$

where $\epsilon_B^{(-\mu,-\nu)} = \epsilon_B^{(\mu\nu)}$ and $\boldsymbol{\mathcal{K}}^{(-\mu,-\nu)} = \boldsymbol{\mathcal{K}}^{(\mu\nu)}$. Using Eqs. (33) and (2) and neglecting the terms of the order ϵ_B^2 and the coupling between harmonics ζ_{mn} with various m, n because of the inhomogeneity of B_0 in the LHS of Eq. (32), we obtain:

$$C^{(s)} = \sum_{m,n,\mu'\nu'} \frac{2i\omega}{c} \nabla \cdot \left(\beta_s \bar{\mathbf{B}} \times \boldsymbol{\mathcal{K}}^{(\mu'\nu')} \zeta_{m+\mu',\, n+\nu' N} e^{im\vartheta - in\varphi} \right), \qquad (34)$$

$$\begin{aligned} \zeta_{m+\mu'\, n+\nu' N} \;=\; & \frac{2ic\omega}{\bar{B}^2 \left(\omega^2 - k^2_{m+\mu',\, n+\nu' N} c_s^2 \right)} \sum_{\mu\nu} \left\{ \left[\bar{\mathbf{B}} \times \boldsymbol{\mathcal{K}}^{(\mu+\mu',\, \nu+\nu')} \right]^r \frac{d\Phi_{m+\mu,\, n+\nu N}}{dr} \right. \\ & + \left. i(m+\mu) \left[\bar{\mathbf{B}} \times \boldsymbol{\mathcal{K}}^{(\mu+\mu',\, \nu+\nu')} \right]^\vartheta \Phi_{m+\mu,\, n+\nu N} \right\}, \end{aligned} \qquad (35)$$

where $k_{m+\mu,\,n+\nu} \equiv [(m+\mu)\iota - (n+\nu N)]/R$.

The denominator in Eq. (35) vanishes when the sound resonance, $\omega^2 = k_\parallel^2 c_s^2$, takes place. Around this resonance, an Alfvén-sound gap in the Alfvén continuum arises when

$$\omega_{A,mn} = \frac{c_s}{R}|(m+\mu)\iota - n - \nu N|, \tag{36}$$

where $\omega_{A,mn}$ is an Alfvén continuum branch with the mode numbers m, n. The gaps with the lowest frequencies are produced by the harmonics of B_0 with $\mu \sim 1$ and $\nu = 0$. Assuming that $\omega_{A,mn} = |m\iota - n|v_A/R$, we conclude that the gaps associated with the mentioned harmonics arise at $\iota \approx n/m$ because $v_A \gg c_s$, in which case Eq. (36) yields $\omega_{A,mn} \approx \mu\iota c_s/R$. Below we show that in reality $\omega_{A,mn}$ may considerably differ from $k_\parallel v_A$. Nevertheless, the conclusion drawn remains valid when $\omega_{A,mn}$ exceeds $k_\parallel v_A$. The presence of non-axisymmetric harmonics ($\nu \neq 0$) provides the fulfillment of Eq. (36) far from the rational surfaces, the corresponding gaps being located in the high frequency part of the spectrum, $\omega \sim N\nu c_s/R$ for $N\nu \gg 1$; in addition, the $\nu \neq 0$ harmonics produce the gaps at low frequencies near rational surfaces located at the plasma periphery where the temperature is low. Note that the waves with the frequencies inside Alfvén-sound gaps are strongly damped (because these waves have the phase velocity about the ion thermal velocity) unless the plasma is non-isothermal with high electron temperature.

Taking into account that $\boldsymbol{\mathcal{K}} = B_0^{-1}\nabla B_0$ (except for the $\mu = 0$, $\nu = 0$ harmonic of $\boldsymbol{\mathcal{K}}$) and $B_\varphi \approx \sqrt{g}B^2 \approx$ const, we obtain:

$$C^{(s)} = \sum_{mn} C_{mn}^{(s)} e^{im\vartheta - in\varphi}, \tag{37}$$

where

$$C_{mn}^{(s)} = -\frac{1}{r}\frac{\partial}{\partial r}\beta_s \sum_{\mu\nu}\left(\chi_{\vartheta\vartheta}^{(\mu\nu)} r\frac{\partial}{\partial r} + m\chi_{r\vartheta}^{(\mu\nu)}\right)\Phi_{m-\mu,n-\nu N}$$
$$+\frac{\beta_s}{r^2}\sum_{\mu\nu}(m+\mu)(m\chi_{rr}^{(\mu\nu)} - \chi_{r\vartheta}^{(\mu\nu)})\Phi_{m-\mu,n-\nu N}, \tag{38}$$

$$\chi_{rr}^{(\mu\nu)} = \sum_{\mu'\nu'}\alpha_{mn}^{(\mu'\nu')}\frac{d\epsilon_B^{(\mu'\nu')}}{dr}\frac{d\epsilon_B^{(\mu+\mu',\,\nu+\nu')}}{dr}, \tag{39a}$$

$$\chi_{\vartheta\vartheta}^{(\mu\nu)} = \frac{1}{r^2}\sum_{\mu'\nu'}\alpha_{mn}^{(\mu'\nu')}\mu'(\mu+\mu')\epsilon_B^{(\mu'\nu')}\epsilon_B^{(\mu+\mu',\,\nu+\nu')}, \tag{39b}$$

$$\chi_{r\vartheta}^{(\mu\nu)} = \frac{1}{r}\sum_{\mu'\nu'}\alpha_{mn}^{(\mu'\nu')}(\mu+\mu')\frac{d\epsilon_B^{(\mu'\nu')}}{dr}\epsilon_B^{(\mu+\mu',\,\nu+\nu')}, \tag{39c}$$

and

$$\alpha_{mn}^{(\mu'\nu')} = \frac{\omega^2}{\omega^2 - k^2_{m+\mu',\,n+\nu' N}c_s^2}. \tag{40}$$

The terms proportional to the temperature gradient are neglected because their contribution is about that produced by the finite plasma pressure, which is not taken into account in our analysis. Note that $\alpha_{mn}^{(\mu,0)} \approx 1$ when $\mu \sim 1$ and $\omega \sim c_s/R$ (or exceeds c_s/R) and $\iota \ll 1$. On the other hand, $\alpha_{mn}^{(\mu\nu)} \ll 1$ for $\omega^2 \ll k^2_{m+\mu,n+\nu N}c_s^2$ with $\nu \neq 0$ (this condition is consistent with the condition $\omega^2 > k^2_{m+\mu,n}c_s^2$ when $N \gg 1$ and/or $\iota \ll 1$). This means that only the $\nu = 0$ terms mainly contribute to the sums in Eq. (39) when ω is well below the high frequency Alfvén-sound gaps.

To proceed further, we write the metric tensor components g^{rr} and $g^{\vartheta\vartheta}$ as[6]

$$g^{rr} = \delta_0\left(1 + \frac{1}{2}\sum_{\mu\nu}\epsilon_g^{(\mu\nu)}e^{i\mu\vartheta - i\nu N\varphi}\right), \quad g^{\vartheta\vartheta} = \frac{\delta_0}{r^2}\left(1 + \frac{1}{2}\sum_{\mu\nu}\epsilon_g^{(\mu\nu)}e^{i\mu\vartheta - i\nu N\varphi}\right), \tag{41}$$

with $\delta_0 \equiv \delta_0(r)$, and neglect the other components of the metric tensor. Note that δ_0 was assumed constant in Ref. 6, which is justified only in the vicinity of the magnetic axis; $\delta_0(r)$ monotonically grows with r, $\delta_0(r) \gtrsim 1$. Due to these expansions, Eq. (30) can be presented as a set of the infinite number of coupled equations for the Fourier harmonics of the scalar potential of the electromagnetic field. The equation for the (m,n)-harmonic coupled with the others can be written as follows:

$$\frac{1}{r}\frac{d}{dr}r\delta_0\left(\frac{\omega^2-\omega_{G1}^2}{v_A^2} - k_{mn}^2\right)\frac{d\Phi_{mn}}{dr} - \left[\frac{m^2\delta_0}{r^2}\left(\frac{\omega^2-\omega_{G2}^2}{v_A^2} - k_{mn}^2\right) + \frac{k_{mn}}{r}(r\delta_0 k'_{mn})'\right]\Phi_{mn}$$
$$+C_{mn}^{(r)} + C_{mn}^{\nabla} - C_{mn}^{(j)} = 0, \tag{42}$$

where $k_{mn} \equiv k_\parallel(m,n) = (m\iota - n)/R$, $C_{mn}^{(r)}$ describes the harmonic coupling due to the terms containing the second radial derivative of the wave function,

$$C_{mn}^{(r)} = \sum_{\mu\nu}\frac{1}{r}\frac{d}{dr}r\delta_0\left[\frac{\omega^2}{v_A^2}\left(\frac{\epsilon_g^{(\mu\nu)}}{2} - 2\epsilon_B^{(\mu\nu)}\right) - k_{mn}k_{m-\mu,n-\nu N}\frac{\epsilon_g^{(\mu\nu)}}{2} - \frac{\omega_{G1}^2}{v_A^2}\epsilon_G^{(\mu\nu)}\right]\frac{d\Phi_{m-\mu,n-\nu N}}{dr}, \tag{43}$$

C^{∇} describes the coupling due to other terms, its part associated with the compressibility is given by Eq. (38) without the terms proportional to $\chi_{\vartheta\vartheta}^{(\mu\nu)}$ and all terms with $\mu = 0$ and

$\nu = 0$; the contribution of the terms with $\mu = 0$ and $\nu = 0$ to Eq. (42) is represented by the frequencies ω_{G1} and ω_{G2} given by

$$\omega_{G1}^2 = \frac{1}{\delta_0} c_s^2 \chi_{\vartheta\vartheta}^{(00)}, \qquad \omega_{G2}^2 = \frac{1}{\delta_0} c_s^2 \chi_{rr}^{(00)}, \tag{44}$$

and $\epsilon_G^{(\mu\nu)} = \chi_{\vartheta\vartheta}^{(\mu\nu)} / \chi_{\vartheta\vartheta}^{(00)}$, with $\mu \neq 0$ and/or $\nu \neq 0$; $C_{mn}^{(j)}$ is a harmonic of $C^{(j)}$. The frequencies ω_{G1} and ω_{G2}, although they are associated with different components of the curvature, are equal in the case of tokamaks. This can also be the case in stellarators, at least, close to the magnetic axis; but, in general, $\omega_{G2} \neq \omega_{G1}$ because the dependence of harmonics of the equilibrium magnetic field on radius is nonlinear.

It follows from Eq. (42) that the local Alfvén resonance is approximately described by the equation (the coupling between Alfvén branches is neglected):

$$\omega^2 = \left(k_\parallel^2 + \frac{\beta_s}{\delta_0} \chi_{\vartheta\vartheta}^{(00)} \right) v_A^2. \tag{45}$$

Note that the RHS of this equation represents the Alfvén continuum in the approximation used.

Let us analyze Eq. (45). We consider first the simplest case of $k_\parallel = 0$ assuming that the equilibrium magnetic field contains only the toroidicity-induced Fourier harmonic, $\epsilon_t \equiv -\epsilon_B^{(10)}$ ($\epsilon_t > 0$). Then Eq. (45) yields:

$$\omega^2 = \omega_G^2 \equiv \frac{2c_s^2}{R^2} \frac{\epsilon_t^2}{\delta_0 \epsilon^2} \left(1 + \frac{\iota^2}{2} \frac{\delta_0 \epsilon^2}{\epsilon_t^2} \right), \tag{46}$$

where $\epsilon = r/R$; typically, $\epsilon_t < \epsilon$ in stellarators. It follows from Eq. (46) that $\omega_G = \sqrt{2}(c_s/R)(1 + \iota^2/2)]$ in tokamaks with circular cross section. The frequency ω_G is associated with the geodesic curvature, $\mathcal{K}_G \equiv 2B^{-1}[\boldsymbol{\mathcal{K}} \times \mathbf{B}] \cdot \nabla r$, as $\omega_G^2 \approx c_s^2 \langle \mathcal{K}_G^2 \rangle$, where $\langle ... \rangle$ means averaging over the angles. Therefore, ω_G is called the "geodesic acoustic frequency". This frequency was introduced for the first time in Ref. 15. It plays an important role in physics of zonal flows and Alfvén cascades in tokamaks.[22,23] However, we should note that introducing ω_G makes sense only provided that the first term in Eq. (46) dominates, i.e., when

$$\mathfrak{S} \equiv \frac{\iota^2}{2} \frac{\delta_0 \epsilon^2}{\epsilon_t^2} \ll 1. \tag{47}$$

In another limit case, $\mathfrak{S} \gg 1$, Eq. (46) describes the sound waves, $\omega^2 = k_\parallel^2 c_s^2$, with $k_\parallel = \iota/R$. We will refer to $\mathfrak{S}$ as a "sound parameter" because, depending on its magnitude, the (m, n) Alfvén continuum branch either avoids the sound resonance (when $\mathfrak{S} \ll 1$) or reaches its

vicinity (when $\mathfrak{S} \gg 1$) at the rational surface $\iota = m/n$. When $\mathfrak{S} \ll 1$, $\omega_s^2/\omega_G^2 \approx \mathfrak{S}$, with $\omega_s = \iota c_s/R$. Equation (47) is typically satisfied in tokamaks, at least, in the region where the safety factor exceeds unity. It is also satisfied in W7-AS discharges with $\iota \ll 1$. In contrast to this, $\mathfrak{S} \gg 1$ in Wendelstein 7-X (W7-X[25]) where $\iota \lesssim 1$ and $\epsilon/\epsilon_t \gtrsim 2.3$, $\delta_0 \sim 1.5$. This implies that ω_G does not exist in W7-X.

We remind that Eq. (46) was obtained by assuming that $\epsilon_B^{(\mu,0)} = 0$ for $\mu \geq 2$. Strictly speaking, this assumption is not justified even for tokamaks. In addition, Eq. (46) was obtained with neglecting the $\nu \neq 0$ terms. Therefore, now we make a more accurate analysis. We write Eq. (45) as follows:

$$\omega^2 \left[1 - \frac{k_{mn}^2 v_A^2}{\omega^2} - F(\omega) \right] = 0, \tag{48}$$

where

$$F(\omega) = \frac{1}{2} \sum_{\mu\nu} \frac{\hat{\epsilon}_{\mu\nu}^2}{\widetilde{\omega}^2 - (\widetilde{k}_{mn} + \widetilde{k}_{\mu\nu})^2} = \frac{\hat{\epsilon}_{10}^2}{\widetilde{\omega}^2 - (\widetilde{k}_{mn} + \widetilde{k}_{10})^2} + \frac{\hat{\epsilon}_{20}^2}{\widetilde{\omega}^2 - (\widetilde{k}_{mn} + \widetilde{k}_{20})^2} + \dots , \tag{49}$$

$\hat{\epsilon}_{\mu\nu} = \sqrt{2/\delta_0}\ \mu\epsilon_B^{(\mu\nu)}/\epsilon$, $\widetilde{\omega} = \omega R/c_s$, $\widetilde{k}_{\mu\nu} = \mu\iota - \nu N$. Equation (48) has the infinite number of solutions. However, only low frequency solutions of Eq. (48) with $k_{mn} = 0$ can satisfy the requirement that the frequency must be beyond the Alfvén-sound gaps. A solution of this kind with $\omega > \iota c_s/R + \Delta_{\rm gap}$, where $\Delta_{\rm gap}$ is the half-width of the lowest Alfvén-sound gap, represents ω_G. For a particular case of $\omega_G > 2\iota c_s/R$ it is shown in Fig. 2. When $3\iota^2 > \hat{\epsilon}_{10}^2$ everywhere in the plasma, $\omega_G < 2\iota c_s/R$. Then $\omega_G(r)$ lies between the $\mu = 1$ Alfvén-sound gap and the $\mu = 2$ gap. Due to this, $\omega_G(r)$ is a continuous function, and the Alfvén continuum with $k_\parallel \neq 0$ exists only above $\omega_G(r)$ and well below the resonance $\omega = \iota c_s/R$. It may happen that $3\iota^2 > \hat{\epsilon}_{10}^2$ only in some plasma region, whereas $3\iota^2 < \hat{\epsilon}_{10}^2$ in the other region (this may happen, in particular, because $\delta_0(r)$ is a growing function). Then, as one can see from Fig. 2, ω_G will have a discontinuity.

Note that an equation for the frequency of the geodesic acoustic mode in arbitrary geometry was presented without derivation in Ref. 26 [Eq. (2) therein]. Like Eq. (46), it contains only two terms, which implies that it neglects the effects described by Eqs. (48) and (49). Therefore, it is of interest to compare Eq. (2) of Ref. 26 and Eq. (46). The notations in Ref. 26 were the same as in Ref. 27. Using this, we found that if we take $m = 1$ and $n = 0$ in Eq. (2) of Ref. 26, the first terms in this equation and Eq. (46) coincide, whereas the

seconds terms differ by a factor of N^2. We conclude that either a factor of N^{-2} is missing in Eq. (2) of Ref. 26 or the notations in Refs. 26 and 27 were different.

Now we consider a particular Alfvén continuum branch with $k_{mn} \neq 0$. It is clear from Eq. (48) that the usual equation for the local Alfvén resonance, $\omega = k_\parallel v_A$, takes place when $F(\omega) \ll 1$. This condition is satisfied at high frequencies, $\omega^2 \gg \omega_G^2$, provided that ω is not close to Alfvén-sound gaps. In addition, it is satisfied at very low frequencies, $\omega^2 \ll \iota^2 c_s^2/R^2$ provided that $\mathfrak{S} \gg 1$, i.e., when the geodesic frequency does not exist. It is interesting to note that Eq. (48) has a solution with $\omega \propto k_\parallel v_A$ at very low frequencies even when $\mathfrak{S} \lesssim 1$ (we used the fact that $F(\omega) \approx -\mathfrak{S}^{-1}$ for $\omega \to 0$):

$$\omega \approx \frac{k_\parallel v_A}{\sqrt{1+\mathfrak{S}^{-1}}}\,. \tag{50}$$

It follows from the foregoing that the character of the Alfvén continuum depends on the sound parameter. Figures 3 and 4, where a particular Alfvén continuum branch ($\omega_{A,mn}$) in the presence of the Alfvén-sound gap is shown for $\mathfrak{S} \gg 1$ and $\mathfrak{S} \ll 1$, demonstrate this. Figure 3 is simpler. It takes into account the presence of only one (toroidal) Fourier harmonic in the equilibrium magnetic field and neglects the plasma inhomogeneity. We observe in Fig. 3 that when $\mathfrak{S} \gg 1$, $\omega_{A,mn} \approx k_{mn} v_A$ everywhere except for the region with ι close to $\iota_{mn} = n/m$, where the branch approaches the sound resonance. In contrast to this, when $\mathfrak{S} \ll 1$, the considered branch lies partly well above the sound resonance, with $d\omega_{A,mn}/dk_\parallel = 0$ at the rational surface, and partly below this resonance, with $d\omega_{A,mn}/dk_\parallel \ll v_A$, in accordance with Eq. (50). Figure 4 presents a picture taking into account the presence of several harmonics of B_0 and plasma inhomogeneity, where, however, details in the vicinity of Alfvén-sound gaps are omitted.

Note that the plasma displacement along the field lines, $\xi_\parallel$, becomes considerable when $F(\omega)$ is not small. To see it, we use Eq. (32) and $\boldsymbol{\xi}_\perp = ic\mathbf{B}_0 \times \nabla\Phi/(\omega B_0^2)$, which give

$$\zeta_{mn} = -2\alpha_{mn}^{(00)} \sum_{\mu\nu} \boldsymbol{\mathcal{K}}^{(\mu\nu)} \cdot \boldsymbol{\xi}_{\perp\, m-\mu}. \tag{51}$$

Then, writing $\boldsymbol{\mathcal{K}} = \sum_{\mu\nu} \boldsymbol{\mathcal{K}}^{(\mu\nu)} \exp(i\mu\vartheta - i\nu N\varphi)$ and assuming that $k_{mn} \to 0$, we obtain from $\xi_\parallel = -(c_s^2/\omega^2)\nabla_\parallel \zeta$ that

$$\xi_{\parallel\, m+\mu,\, n+\nu N} = \frac{2ic_s^2 k_{\mu\nu}}{\omega^2 - k_{\mu\nu}^2 c_s^2} \sum_{\mu'\nu'} \boldsymbol{\mathcal{K}}^{(\mu'\nu')} \cdot \boldsymbol{\xi}_{\perp\, m+\mu-\mu',\, n+\nu N-\nu' N}. \tag{52}$$

In particular, Eq. (52) yields $\xi_{\parallel\, m+1,n}/\xi_{\perp\, m,n} \sim \iota\delta_0\epsilon/\epsilon_t$ when $\omega = \omega_G$ and the curvature harmonic with $\mu = 1$ and $\nu = 0$ dominates. For $\omega \ll c_s\iota/R$, we obtain $\xi_{\parallel\, m+1,n}/\xi_{\perp\, m,n} \sim \iota^{-1}\epsilon_t/\epsilon$. Thus, $\xi_\parallel$ is negligible only for $\iota^{-1}\epsilon_t/\epsilon \ll 1$ (in which case $\mathfrak{S} \gg 1$), as one could expect. This implies that continuum branches and discrete modes are actually hybrid Alfvén-sound oscillations when they are close to the flux surfaces where $\iota = n/m$ with m and n the mode numbers, except for the case of $\mathfrak{S} \gg 1$ with $\omega \ll \iota c_s$.

Let us consider the influence of the compressibility on the gaps in the Alfvén continuum. First of all, as was already mentioned, the compressibility leads to the appearance of the Alfvén-sound gaps. Because of the presence of non-axisymmetric harmonics of B_0 in stellarators, these gaps exist even at rather high frequencies, $\omega \sim \nu N c_s/R$, although their width is rather narrow because, first, $\epsilon_B^{(\mu\nu)}$ are small for large μ, ν, and second, the Alfvén-sound gaps are determined by $\epsilon_B^{(\mu\nu)}$, which typically are much less than $\epsilon_g^{(\mu\nu)}$.

In addition, the compressibility changes the frequencies of the gaps existing in incompressible plasmas. Below we consider this effect.

It is clear that the presence of the term proportional to the temperature in Eq. (45) affects the continuum branches. This term, in contrast to the first term, typically decreases with the radius. This promotes the existence of gap modes in the case when the gap is "closed" at the edge because of the small particle density in this region.

Assuming that two cylindrical continuum branches with the mode numbers m, n and $m+\mu$, $n+\nu N$ intersect at a point r_1, we write $k_{mn}(r_1) = -k_{m+\mu,n+\nu N}(r_1)$ and restrict ourselves to the consideration of the interaction between the wave functions with the mentioned mode numbers. In addition, we assume that $k_{mn}^2 v_A^2 \gg \omega_{G1}^2$. This condition is satisfied for the toroidicity-induced gap (which lies below the other gaps and, thus, is affected by the compressibility more than the other gaps) when

$$\frac{\omega_{G1}^2}{\omega_{\rm TAE}^2} = \frac{4\beta_s}{\iota^2\delta_0}\chi_{\vartheta\vartheta}^{(00)}R^2 \sim \frac{4\beta_s}{\iota^2} \ll 1, \tag{53}$$

where $\omega_{\rm TAE}$ is a characteristic frequency of the TAE gap, $\omega_{\rm TAE} = 0.5\iota v_A/R$. Finally, we assume that there are no Alfvén-sound gaps in the vicinity of the considered Alfvén gap and that the Alfvén gap is narrow. In this approximation, $\omega_{G1} \approx \omega_G$ and we can take ϵ_G at the frequency at which the considered cylindrical branches intersect. Then, using Eq. (42) for Φ_{mn} and $\Phi_{m+\mu,n+\nu N}$, we obtain:

$$\omega_\pm^2 = k_{mn}^2 v_A^2[1 \pm (\epsilon_g - 2\epsilon_B)] + \omega_{G1}^2(1 \mp \epsilon_G)\left[1 \pm (0.5\epsilon_g - 2\epsilon_B)\right], \tag{54}$$

where the upper/lower sign refers to the upper/lower boundary of the gap, all the magnitudes are taken in the intersection point of the two cylindrical branches, and the superscripts μ and ν at ϵ_g, ϵ_B, and ϵ_G are omitted. This leads to the gap width

$$\Delta\omega \equiv \omega_+ - \omega_- = \frac{1}{\omega_+}\left[k_{mn}^2 v_A^2(0.5\epsilon_g - \epsilon_B) + \omega_{G1}^2(0.25\epsilon_g - \epsilon_B - 0.5\epsilon_G)\right] \tag{55}$$

and ω_+, ω_- given by

$$\omega_\pm = k_{mn} v_A \left\{1 \pm (0.5\epsilon_g - \epsilon_B) + \frac{\omega_{G1}^2}{2k_{mn}^2 v_A^2}(1 \mp \epsilon_G)[1 \pm (0.5\epsilon_g - 2\epsilon_B)]\right\}. \tag{56}$$

It follows from Eq. (55) that the compressibility increases or decreases the gap width, depending on the sign of the coefficient at ω_{G1}^2, i.e., the sign of $(0.25\epsilon_g - \epsilon_B - 0.5\epsilon_G)$. As we already mentioned, typically $\epsilon_g \gg \epsilon_B$ in stellarators because of strong plasma shaping. Therefore, the effect is determined mainly by competition between the ϵ_g term and the ϵ_G term. Effects of compressibility on the gap boundary can be different, as is seen from Eq. (56). In the limit case of $\epsilon_G \ll 1$, both the upper edge and the lower edge of the gap are shifted up, the upper edge being shifted stronger. In contrast to this, the upper edge is not changed by the compressibility, whereas the lower one is strongly up-shifted when $\epsilon_G \to 1$.

Equation (42) can be written in the Schrödinger form given by Eq. (9) with the potential energy $G(r)$ if the coupling between harmonics is neglected. For currentless stellarators the potential energy can be written as follows:

$$G^S(r) = \frac{m^2}{r^2}\frac{P_2}{P_1} - \frac{1}{4r^2} - \left(\frac{P_1'}{2P_1}\right)^2 + \frac{1}{2r}\frac{P_1'}{P_1} + \frac{P_1''}{2P_1} - \frac{k_\parallel(\delta_0 r k_\parallel')'}{rP_1}, \tag{57}$$

where $P_{1,2} = \delta_0\left(\omega_{A1,2}^2 - \omega^2\right)/v_A^2$, with $\omega_{A1,2}^2 = k_\parallel^2 v_A^2 + \omega_{G1,2}^2$. To obtain $G(r)$ in tokamaks with including effects of the compressibility, one should put $\nu_\iota = 1$ in Eq. (10) and replace ω^2 with $\omega^2 - \omega_{G1}^2$ in all the terms of this equation. We remind that a condition of the existence of eigenmodes is given by Eq. (11).

When $\omega_{G1,2}$ weakly depends on ω and the modes are well-localized, we can, as in Sec. II, transform the equation $d^2Y/dr^2 - G(r)Y = 0$ to other Schrödinger-type equations, where a key parameter is g given by

$$g^S = \frac{2v_A^2}{(\omega_{A1}^2)''}\left\{\frac{mk_\parallel\iota'}{rR}\left[\delta_0\left(1 + \frac{r\iota''}{\iota'}\right) + r\delta_0'\right] - \frac{m^2}{r^2}\frac{\omega_{G2}^2 - \omega_{G1}^2}{V_A^2}\right\}, \tag{58}$$

$$g^T = -\frac{4v_A^2}{(\omega_{A1}^2)''}\frac{mk_\parallel\iota'}{rR}, \tag{59}$$

with

$$(\omega_{A1}^2)'' = 2k_\parallel^2 v_A^2 \left[\frac{k_\parallel'^2}{k_\parallel^2} + \frac{k_\parallel''}{k_\parallel} - \frac{\rho''}{2\rho} + \frac{\omega_{G1}^2}{k_\parallel^2 v_A^2} \left(\frac{\rho'}{\rho}\frac{T'}{T} + \frac{T''}{2T} \right) \right], \tag{60}$$

and all the magnitudes are taken at the point determined by $(\omega_{A1}^2)' = 0$, i.e.,

$$\frac{2m\iota'}{k_\parallel R} - \frac{\rho'}{\rho} + \frac{\omega_{G1}^2}{k_\parallel^2 v_A^2}\frac{T'}{T} = 0. \tag{61}$$

In the case when $\iota' \approx 0$ in the vicinity of the point determined by Eq. (61) with the term proportional to ι' neglected, we obtain:

$$g^S = \frac{\delta_0 m k_\parallel r^2 \iota'' v_A^2 - m^2 R(\omega_{G2}^2 - \omega_{G1}^2)}{m k_\parallel r^2 \iota'' v_A^2 + \left(\frac{\rho' T'}{\rho T} + \frac{T''}{2T} - \frac{T'\rho''}{2T\rho'} \right) r^2 R \omega_{G1}^2}. \tag{62}$$

It follows from this equation that $g^s = \delta_0$ when the first terms in the numerator and denominator dominate. The effect of finite ω_{G1} and ω_{G2} depends on profiles of plasma parameters.

The analysis above ignores effects associated with gradient of the plasma pressure. In order to see the limit of validity of this approach, we add the pressure gradient term $8\pi\nabla \cdot (I\mathbf{B}_0 \times \boldsymbol{\mathcal{K}})$, with $I = (\mathbf{B}_0 \times \nabla p) \cdot \nabla\widetilde{\Phi}/B_0^4$, to Eq. (30).[21] It is clear that this term, first, directly contributes to the equation for a certain Fourier harmonic Φ_{mn} and, second, leads to additional coupling between different Fourier harmonics. Let us first neglect the coupling. Then the ∇p-term can be written as $8\pi \sum_{mn} (m^2/r^2)(\delta_0/v_A^2)\omega_P^2 \Phi_{mn} \exp(-i\omega t - in\varphi + im\vartheta)$, where

$$\omega_P^2 = -\frac{2C}{\delta_0}\frac{p'}{\rho}\overline{\mathcal{K}}_r, \tag{63}$$

$C = 1$, $\overline{\mathcal{K}}_r$ is the average radial component of the curvature, $p' = dp/dr$. If we assume that $\epsilon_B^{(00)} \sim \epsilon^2$ and $\epsilon_B^{(\mu\nu)} \sim \epsilon$ for μ or $\nu \neq 0$, the quantity $\overline{\mathcal{K}}_r$, like in tokamaks, can be estimated as $\overline{\mathcal{K}}_r \sim \epsilon\sigma/R$ with $\sigma \sim 1$.[23,28] Thus, $\overline{\mathcal{K}}_r$ is less than the non-averaged curvature by a factor of ϵ; therefore, the coupling terms are of the order of those containing the average curvature. Due to this, the resulting effect of ∇p on the modes can be qualitatively described by taking $C \neq 1$ in Eq. (63). Note that the coupling may change the sign of C. To incorporate ω_P^2 into the equations derived above [Eq. (42), (58), (62)], one has to replace ω_{G2}^2 with the sum $\omega_{G2}^2 + \omega_P^2$. It follows from here that the effects of ∇p can be disregarded when $\omega_P^2 \ll \omega_G^2$, which leads to

$$rp' \ll p \tag{64}$$

in the region where the mode is localized, which is true for core-localized modes. Moreover, one can see from Eq. (58) with the added ∇p-term that the influence of ∇p on NGAEs in

stellarators may be not important even when Eq. (64) is not satisfied. This is the case for NGAEs with sufficietly large longitudinal wave numbers:

$$k_{\parallel}R \gg \frac{m}{r^2\iota''}\frac{\beta}{\delta_0}\frac{d\ln p}{d\ln r}. \tag{65}$$

In order to calculate eigenmodes with taking into account effects of plasma compressibility included to Eq. (42), the code BOA (Branches Of Alfvén modes)[6] was extended and a new code BOA-fe (BOA – finite elements) finding eigensolutions with higher accuracy was developed. In addition, the code COBRAS (COntinuum BRanches of Alfvén and Sound waves)[24] calculating the MHD continuum was amended to make the identification of specific Alfvén and sound branches of the continuum, as well the calculation of the boundaries of continuum gaps, possible.

IV. MODELING OF LOW FREQUENCY ALFVÉNIC ACTIVITY IN WENDELSTEIN 7-AS

Low frequency instabilities were observed in all W7-AS discharges with Alfvénic activity driven by the neutral beam injection (NBI). We selected the discharge #39029, in which several modes with $m = 3$ in the frequency range of $30 - 40$ kHz and an $m = 5$ mode with the frequency of $\lesssim 50$ kHz were destabilized simultaneously, as shown in Fig. 5. In this discharge, the Alfvénic activity had a quasi-steady-state character; it had maximum amplitudes at $r/a \sim 0.3 - 0.5$ and occupied a rather wide region. The available equilibrium data are relevant to $t = 0.45$ s. At this time, the most pronounced signals had the frequencies of 33 kHz, 35 kHz, and 38 kHz, all relevant to $m = 3$ modes, and 46 kHz, relevant to an $m = 5$ mode. The injected power was rather low, $P_{\rm inj} = 440$ kW, and the Alfvén velocity was large (small $P_{\rm inj}$ led to low plasma density limit), which may explain why high frequency Alfvén instabilities were absent. This conclusion can be drawn from a simple equation for the driving part of the instability growth rate (γ_α), which indicates that typically $\gamma_\alpha^{LF} > \gamma_\alpha^{HF}$ (the superscripts "LF" and "HF" are relevant to low-frequency instabilities and high frequency instabilities, respectively) for given parameters. To see it, we write the following estimate for the growth rate (expressions for the growth rate obtained in Refs. 5,29 are used):

$$\gamma_\alpha \propto \frac{\alpha_v^4 P_{\rm inj} T_e^{3/2}}{\alpha_\omega^2 M_i^2 n_e^3 \iota} \tag{66}$$

where $P_{\rm inj}$ is the injected NBI power, α_ω characterizes the mode frequency being defined by $\omega = \alpha_\omega v_A/R$, and α_v determines the resonance velocity of the injected particles, $v_\parallel^{\rm res} = \alpha_v v_A$. In the considered discharge $\alpha_v < 1$ and $P_{\rm inj}$ was small, therefore, γ_α was small, too, except for the case of $\alpha_\omega \ll 1$. Of course, Eq. (66) is rough, but, nevertheless, it agrees with W7-AS experiments showing the presence of HF-instabilities only in the discharges with $P_{\rm inj} > 1$ MW. Note that when $k_\parallel \to 0$, so that $\omega \to \omega_G$, γ_α decreases because in this case the resonance velocity is much less than v_A even when the injection velocity, v_α, exceeds v_A. In particular, when the mode is destabilized through the toroidicity-induced sideband resonance, $v^{\rm res} \to \pm\omega_G R/\iota \sim \pm c_s/\iota$.

The important parameters of the considered discharge are the following: the equilibrium magnetic field is $\bar{B} = 2.53$ T, the electron density is $n_e(0) = 1.1 \times 10^{14}$ cm^{-3}, the plasma temperature is $T(0) = 540$ eV, the plasma radius is $a = 17$ cm, and the edge rotational transform is $\iota_a = 0.35$. A deuterium plasma but hydrogen NBI were used. The radial profiles of plasma parameters are shown in Fig. 6. Fourier harmonics of the equilibrium magnetic field and the radial profiles of plasma parameters are shown in Fig. 7. The magnetic shear was very low.

Before analyzing the experimental data, we note that GAE/NGAE modes with $k_\parallel R \ll 1$ are extremely sensitive to the magnitude of the rotational transform, especially when $m \gg 1$. A small change of ι or the ι error bar may have a largest effect when more than one mode is destabilized simultaneously. This will be the case when the waves are localized approximately in the same region and propagate in opposite directions along the magnetic field, i.e., $\mathrm{sgn}\, k_{m_1,n_1} = -\mathrm{sgn}\, k_{m_2,n_2}$ (note that this condition does not contradict to the fact that the waves destabilized by the spatial inhomogeneity of the energetic ions propagate in the same direction along the large azimuth of the torus, $\mathrm{sgn}\, n_1 = \mathrm{sgn}\, n_2$). Then the most sensitive quantity is the difference between the mode frequencies ($\omega_2 - \omega_1$, with $\omega_{1,2}$ the frequency of the mode with the mode numbers $m_{1,2}$ and $n_{1,2}$):

$$\Delta|\omega_2 - \omega_1| = |m_1 + m_2|\Delta\iota\frac{v_A}{R}, \tag{67}$$

where $\Delta\iota$ is the change of ι or the ι error bar, and all the quantities are taken at the point r_0 where the mode amplitude is maximum. In particular, for the considered discharge with $m_1 = 3$ and $m_2 = 5$, this yields $\Delta\iota \cdot 2400$ kHz in a deuterium plasma (and more in the presence of protons); for instance, a very small error in determination of ι, $\Delta\iota = 0.001$,

leads to an error of 2.4 kHz! Note that the sensitivity of the frequency to ι is strong even if the waves propagate in the same direction; in the considered case the frequency error would decrease only by a factor of $|m_1 + m_2|/|m_1 - m_2| = 4$. It is clear that the codes calculating equilibrium configurations cannot provide $\iota(r)$ with so high accuracy (because of the presence of the bootstrap current, beam-induced current, Ohmic current etc). To evaluate the influence of the iota error bar on the single frequency, we have to take either $m_1 = 0$ or $m_2 = 0$ in Eq. (67). The influence of $\Delta\iota$ on the gap modes is different. Because the mode numbers determine both the gap frequency and $\iota(r_0)$, a change of iota leads to a change of r_0 ($\Delta\iota \approx \iota' \Delta r_0$) or the mode numbers ($\Delta\iota = \Delta[(2n + \nu N)/(2m + \mu)]$) when r_0 does not change. In the latter case, the mode frequency also changes. In particular, for the TAE modes we have:

$$\Delta\omega^{\mathrm{TAE}} = \frac{\Delta\iota}{2}\frac{v_A}{R}. \tag{68}$$

We observe that the TAE frequency is less sensitive to $\Delta\iota$ than the GAE/NGAE frequency by a factor of $2m$. Equations (67) and (68) were obtained in the assumption that $\omega = k_\parallel v_A$. Taking into account finite ω_G decreases the influence of $\Delta\iota$ on the frequency by a factor of $(1 + \omega_G^2/\omega_A^2)^{1/2}$.

Note that emergence of Alfvén grand cascades, when modes with various n appeared simultaneously, was used in JET to conclude that the minimum of the safety factor was at a rational flux surface.[13]

It follows from what was said that $\iota(r)$ obtained in equilibrium calculations can hardly be used for calculation of the GAE/NGAE mode structure and, in some cases, even for identification of the instability. Instead, an analysis of experimentally observed characteristics of the modes can be used for a reconstruction of the iota profile, or at least, determination of ι in certain points. Below we demonstrate this.

Basing on Fig. 5, we require that $\iota(r)$ should provide the following:

(i) At least, three eigenmodes with $m = 3$ and various frequencies must exist, such that $\omega_{\max} - \omega_{\min} = 5$ kHz; the mode with $\omega_{\min}$ should be located closer to the magnetic axis than the mode with $\omega_{\max}$. This implies that Alfvén continuum of the $m = 3$ branch must have two extrema, a minimum and a maximum. The minimum should be located closer to the magnetic axis, and the difference between the maximum magnitude and the minimum magnitude of the continuum frequency must be a little less than 5 kHz.

(ii) The frequency of the $m = 5$ mode should exceed the maximum frequency of the

$m = 3$ mode by ~ 9 kHz.

(iii) The maximum of the wave function of the $m = 3$ mode with the lowest frequency, 33 kHz, should be located at $r/a \sim 0.3$. The maxima of the other modes should be located at $r/a \sim 0.4 - 0.5$.

(iv) The reconstructed $\iota(r)$ must be in reasonable agreement with that obtained in equilibrium calculations; in particular, the edge rotational transform should be considered as a given quantity, $\iota_a \approx 0.35$.

In the considered discharge hydrogen was injected into a deuterium plasma. Because of this, plasma consisted of the mixture of deuterium and hydrogen. The mode frequency is proportional to $1/\sqrt{M_i}$, where $M_i = M_H(2 - \nu_H)$, where M_H is the proton mass, M_i is the effective ion mass, and $\nu_H \equiv n_H/n_i$ is the fraction of hydrogen, $0 < \nu_H < 1$. The magnitude of ν_H was not known from the experiment. However, it can be exactly determined due to simultaneous observation of the $m = 3$ mode and the $m = 5$ mode. Indeed, we have two equations for the modes localized approximately around the same radius, $\omega_1 = f_1(m_1, M_i, \iota_*)$ and $\omega_2 = f_2(m_2, M_i, \iota_*)$, and two variables, M_i and $\iota_* = \iota(r_*)$, with $r_*/a \approx 0.5$ the point where the amplitudes of the $m = 3$ mode with the frequency of 38 kHz and the $m = 5$ mode have maxima.

A simple estimate shows that $\omega_G \sim 20$ kHz in the core of a deuterium plasma and 28 kHz in a hydrogen plasma. This implies that the compressibility does not prevent from the existence of the modes with experimentally observed frequencies ($\omega > 28$ kHz). On the other hand, $20 - 28$ kHz is comparable with the observed frequencies. Therefore, the influence of the plasma compressibility on the modes is rather strong, and thus, the compressibility must be taken into account in calculations. Simple estimates of the mode frequencies show that $n = 1$ when $m = 3$ and $n = 2$ for $m = 5$. Using these mode numbers, we calculated the corresponding continuum branches by the code COBRAS, varying $\iota(r)$ and M_i in order to satisfy the formulated above constraints. After that, the selected magnitudes were tested and slightly varied again to calculate the eigenmodes. This was done by the code BOA. It was shown by BOA that there are several eigenmodes above the maximum of the $m/n = 3/1$ continuum branch, the highest frequency being above the continuum by about 1.5 kHz in deuterium, whereas the other modes have the frequencies very close to extrema of the continua. Using these facts, the final choice of ι and M_i was done and the full picture of the low frequency part of the continuum was calculated. The continuum and the

eigenmodes for $M_i = 1.39 M_H$ ($\nu_H = 60\%$) are shown in Fig. 8 and Fig. 9, respectively. The rotational transform reconstructed by using results of calculations of the Alfvén continuum and eigenmodes is shown in Fig. 10 by the solid lines. In addition, the upper dashed curve in Fig. 10 represents $\iota(r)$ calculated with neglecting the plasma currents by the code VMEC.[14] The lower dashed curve shows the results of the VMEC calculation corrected by adding evaluated effects of the bootstrap current, j_b, and the Ohmic heating current, $j_{\rm OH}$, but the beam-driven current, $j_{\rm NBI}$, is still neglected (although injection was non-balanced and, thus, this current was considerable). The current $j_{\rm OH}$ was used to compensate other currents, so that $j_{0\|} = j_{\rm NBI} + j_b - j_{\rm OH}$, and $\int_0^a j_{0\|}\, r\, dr \approx 0$. It is clear, however, that this integral condition, even if it is satisfied exactly, cannot provide vanishing of the local plasma current. Furthermore, this condition implies that $j_{0\|}$ has different signs on different radii because partial currents $j_{\rm NBI}$, j_b, and $j_{\rm OH}$ have different radial dependences. Due to this and to the fact that $\iota_{\rm ext}(r)$ is very flat, the resulting $\iota(r)$ may have a complicated radial dependence, which makes plausible $\iota(r)$ shown by solid curves. On the other hand, we have to note that, as shown above, one can use observations of instabilities to reconstruct ι with high accuracy at several characteristic points (in particular, at extrema of continuum branches); however, the ι profile away from these points can be reconstructed only with some uncertainty.

It follows from our analysis that the instability with $m = 5$ can be identified as a destabilized GAE mode, whereas the instabilities with $m = 3$ represent a combination of GAE and NGAE modes.

V. SUMMARY AND CONCLUSIONS

The paper contains both a general theory of the GAE/NGAE modes in stellarator plasmas and a consideration of a particular W7-AS discharge in which low-frequency Alfvén instabilities were observed. The obtained results can be summarized as follows.

Equations describing the GAE/NGAE modes in stellarator plasmas are derived. Conditions of the existence of the GAE/NGAE modes have been obtained. They are actually the conditions of the existence of the potential well in a Schrödinger-type equation that approximately describes eigenmodes. These conditions are very different in plasmas with and without the local toroidal current, which implies that the GAE/NGAE modes which exist when the rotational transform, ι, is produced by the plasma current may not exist

when ι is produced by the external coils and vice versa. In the cold plasma approximation, the obtained conditions are well satisfied in currentless stellarators with non-monotonic $\iota(r)$ when the mass density, ρ, is flat in the region of the mode localization, whereas they are not satisfied in tokamaks. This result implies that NGAE modes can be most easily observed in currentless stellarators with flat $\rho(r)$. On the other hand, this explains why taking into account various factors (such as the presence of the energetic ions, toroidal effects, gradients of the plasma pressure) is necessary to explain observations of RSAE modes responsible for the Alfvén cascades in tokamaks.

The effects of plasma compressibility were also studied. It is found that the plasma compressibility can play an important role. It prevents the existence of the NGAE modes with frequencies $\omega < \omega_G$, although Alfvén modes coupled with sound waves may still exist at very low frequencies, $\omega < \iota c_s/R$. In other words, there is a "forbidden zone" in the Alfvén spectrum, $\iota c_s/R < \omega < \omega_G$, where NGAE modes cannot exist. Below this zone, $\omega < \iota c_s/R$, the situation is more complicated because of effects which cannot be described by ideal MHD. Note that the geodesic acoustic frequency in stellarators differs from that in tokamaks because of the presence of many Fourier harmonics in the equilibrium magnetic field, $\epsilon_t < r/R$, and strong plasma shaping. All these factors reduce the effects of compressibility in stellarators except for the case when the mode frequency approaches an Alfvén-sound resonance associated with the presence of non-axisymmetric Fourier harmonics of the magnetic field. The presence of these harmonics makes Alfvén-sound resonances possible not only at very low frequencies but also when $\omega \sim \omega_{\rm TAE}$, in which case these resonances occur at the plasma edge where the temperature is much lower than in the plasma core. It is shown that features of the Alfvén spectrum when ι is close to rational surfaces can be different. A key parameter [$\mathfrak{S}$ given by Eq. (47)] which determines these features is found. The geodesic frequency exists only when $\mathfrak{S} \ll 1$. In stellarators, this parameter can vary in a wide range. In particular, $\mathfrak{S} \ll 1$ in W7-AS discharges with $\iota \ll 1$, whereas $\mathfrak{S} \gg 1$ in W7-X. Thus, from this point of view, W7-AS and W7-X are qualitatively different devices.

The compressibility affects Alfvén modes through coupling of Alfvén and sound harmonics of the perturbation because of the inhomogeneity of the magnetic field (described by ϵ_B). In addition, there is a coupling between Alfvén harmonics themselves due to both the inhomogeneity of B and plasma shaping (described by ϵ_g). The former coupling influences the continuum and the mode frequency as described above. The latter coupling was neglected

in this work. One can expect that its main effect is the continuum damping, which arises when the frequency of the main harmonic intersects the continuum branches of sideband harmonics.

We draw attention to the fact that the low-frequency GAE/NGAE modes are much more sensitive to the ι profile than the gap modes. This means that experimental observations of these modes can be used for a very precise reconstruction of $\iota(r)$. This statement is general, i.e., it is relevant to any toroidal device with any profile of the rotational transform. Especially favorable for the reconstruction of $\iota(r)$ is the situation when several modes are destabilized simultaneously. Just this was the case in the W7-AS discharge #39029, in which an $m = 5$ mode and several $m = 3$ modes were destabilized. Therefore, this discharge was selected for modeling in this paper. Both Alfvén continua and eigenmodes were calculated for various $\iota(r)$, which enabled to find $\iota(r)$ that gives the best agreement with experimental observations of Alfvénic activity. Moreover, the analysis carried out enabled us to make a conclusion on the fraction of the hydrogen and deuterium in the plasma. We identified the $m = 5$ mode as a GAE with $n = 2$, and the $m = 3$ modes as a GAE and a NGAE with $n = 1$.

Note that the conditions for getting several GAE modes are not known, but it was very typical to see two lines and sometimes more lines in the spectrum. The occurrence of several modes does not seem to depend on a certain mixture of H and D (as expected for MHD modes). Therefore, our results are equally applicable to cases with only one ion species.

However, we cannot claim that the reconstructed profile of $\iota(r)$ really coincides with the profile that took place in the experiment because of the lack of experimental data on plasma rotation. Thus, our analysis of the selected discharge should be considered as a demonstration of the potential to use low frequency instabilities for diagnostics in stellarators. In addition, this analysis showed that plasma compressibility may play an important role in low frequency Alfvén instabilities occurring in stellarators.

The calculations of the Alfvén continuum were carried out by the code COBRAS, whereas the eigenmodes were calculated by a new code, BOA-fe (Branches Of Alfvén – finite elements), solving an equation for Alfvén eigenmodes, such as GAE and NGAE modes, with higher accuracy and with taking into account the plasma compressibility. The necessity of the development of this code was caused by the facts that, first, the potential well responsible for GAE and NGAE can be very shallow, and second, the plasma compressibility may

play an important role. The previous finite difference code, BOA, often failed to find the eigenmodes in this case. The new code employs a finite-element numerical approximation. The current versions of the code use quadratic and cubic finite elements, but in the case of necessity the code can be extended to higher orders. This allows performing calculations with a smaller number of radial grid points but with higher accuracy as compared to the finite-difference approximation.

In conclusion, it follows from this paper that predictive calculations of Alfvén instabilities in future devices (in particular, in Wendelstein 7-X) are justified only for the gap modes. Predictive calculations of low frequency GAE/NGAE modes cannot be reliable because equilibrium calculations can hardly provide knowledge of $\iota(r)$ with required accuracy [because these modes are very sensitive to $\iota(r)$]. On the other hand, observations of low frequency Alfvénic activity and plasma rotation can be used for plasma diagnostics, in particular, they can help to reconstruct $\iota(r)$.

Acknowledgments

The work is carried out within the Partner Project Agreement P-034f between Science and Technology Center in Ukraine, Institute for Nuclear Research, and Max-Planck-Institut für Plasmaphysik. One of the authors (Ya.K.) also acknowledges support by the International Bureau of the Federal Ministry of Education and Research (BMBF) at DLR in the frame of the Co-Operation Project WTZ-UKR 06/005. The authors thank P. Helander for reading the manuscript and his comments.

---

[1] King-Lap Wong, Plasma Phys. Control. Fusion **41**, R1 (1999).

[2] A. Weller, M. Anton, J. Geiger, M. Hirsch, R. Jaenicke, A. Werner, W7-AS Team, C. Nührenberg, E. Sallander, and D. A. Spong, Phys. Plasmas **8**, 931 (2001).

[3] K. Toi, S. Yamamoto, N. Nakajima *et al.*, Plasma Phys. Control. Fusion **46**, S1 (2004).

[4] J. P. Goedbloed, H. A. Holties, S. Poedts, G. T. A. Huysmans, and W. Kerner, Plasma Phys. Control. Fusion **35**, B277 (1993).

[5] Ya. I. Kolesnichenko, V. V. Lutsenko, H. Wobig, and Yu. V. Yakovenko, Phys. Plasmas **9**, 517 (2002).

[6] Ya. I. Kolesnichenko, V. V. Lutsenko, H. Wobig, Yu. V. Yakovenko, and O. P. Fesenyuk, *IPP Report III/261* (Max-Planck-Institut für Plasmaphysik, Garching bei München, 2000); Phys. Plasmas **8**, 491 (2001).

[7] C. Nührenberg, in *ISSP-19 "Piero Caldirola", Theory of Fusion Plasmas*, edited by J. W. Connor, O. Sauter, and E. Sindoni (Editrice Compositori – Società Italiana di Fisica, Bologna, 2000), p. 313.

[8] N. Nakajima, C. Z. Cheng, and M. Okamoto, Phys. Fluids B **4**, 1115 (1992).

[9] Ya. I. Kolesnichenko, V. V. Lutsenko, A. Weller, A. Werner, H. Wobig, Yu. V. Yakovenko, J. Geiger, and S. Zegenhagen, Nucl. Fusion **46**, 753 (2006).

[10] Yu. V. Yakovenko, A. Weller, A. Werner, S. Zegenhagen, O. P. Fesenyuk, and Ya. I. Kolesnichenko, Plasma Phys. Control. Fusion **49**, 535 (2007).

[11] K. Appert, R. Gruber, F. Troyon, and J. Vaclavik, Plasma Phys. **24**, 1147 (1982).

[12] Ya. I. Kolesnichenko, Yu. V. Yakovenko, A. Weller, A. Werner, J. Geiger, V. V. Lutsenko, and S. Zegenhagen, Phys. Rev. Lett. **94**, 165004 (2005).

[13] S. E. Sharapov, B. Alper, H. L. Berk *et al.*, Phys. Plasmas **9**, 2027 (2002).

[14] S. P. Hirshman and D. K. Lee, Comput. Phys. Commun. **39**, 161 (1986).

[15] N. Winsor, J. L. Johnson, and J. M. Dawson, Phys. Fluids **11**, 2448 (1968).

[16] S. M. Mahajan, D. W. Ross, and G. L. Chen, Phys. Fluids **26**, 2195 (1983).

[17] O. S. Burdo, O. K. Cheremnykh, S. M. Revenchuk, and V. D. Pustovitov, Plasma Phys. Control. Fusion **36**, 641 (1994).

[18] H. L. Berk, D. N. Borba, B. N. Breizman, S. D. Pinches, and S. E. Sharapov, Phys. Rev. Lett. **87**, 185002 (2001).

[19] B. N. Breizman, H. L. Berk, M. S. Pekker, S. D. Pinches, and S. E. Sharapov, Phys. Plasmas **10**, 3649 (2003).

[20] S. V. Konovalov, A. B. Mikhailovskii, M. S. Shirokov, and T. Ozeki, Phys. Plasmas **11**, 2303 (2004).

[21] O. P. Fesenyuk, Ya. I. Kolesnichenko, H. Wobig, and Yu. V. Yakovenko, Phys. Plasmas **9**, 1589 (2002).

[22] A. Kramer-Flecken, S. Soldatov, H. R. Koslowski, and O. Zimmermann, Phys. Rev. Lett. **97**, 045006 (2006).

[23] G. Y. Fu and H. L. Berk, Phys. Plasmas **13**, 052502 (2006).

[24] O. P. Fesenyuk, Ya. I. Kolesnichenko, H. Wobig, and Yu. V. Yakovenko, Scientific Papers of the Institute for Nuclear Research (Special Issue: papers from the International Workshop "Innovative Concepts and Theory of Stellarators", Kyiv, Ukraine, 28-31 May 2001), Kyiv, ISSN 1606-6723, No. 4(6), p. 105 (2001).

[25] G. Grieger, Nucl. Fusion Suppl. **3**, 525 (1991).

[26] C. Nührenberg and K. Hallatschek, in *33rd European Physical Society Conference on Plasma Physics, Rome, 2006*, Europhysics Conference Abstracts, Vol. 30I (European Physical Society, Petit-Lancy, 2006), Report P-2.116.

[27] C. Schwab, Phys. Fluids B **5**, 3195 (1993).

[28] Ya. I. Kolesnichenko, R.B. White, Yu. V. Yakovenko, Phys. Plasmas **10**, 1449 (2003).

[29] Ya. I. Kolesnichenko, S. Yamamoto, K. Yamazaki, V. V. Lutsenko, N. Nakajima, Y. Narushima, K. Toi, and Yu. V. Yakovenko, Phys. Plasmas **11**, 158 (2004).

Figures

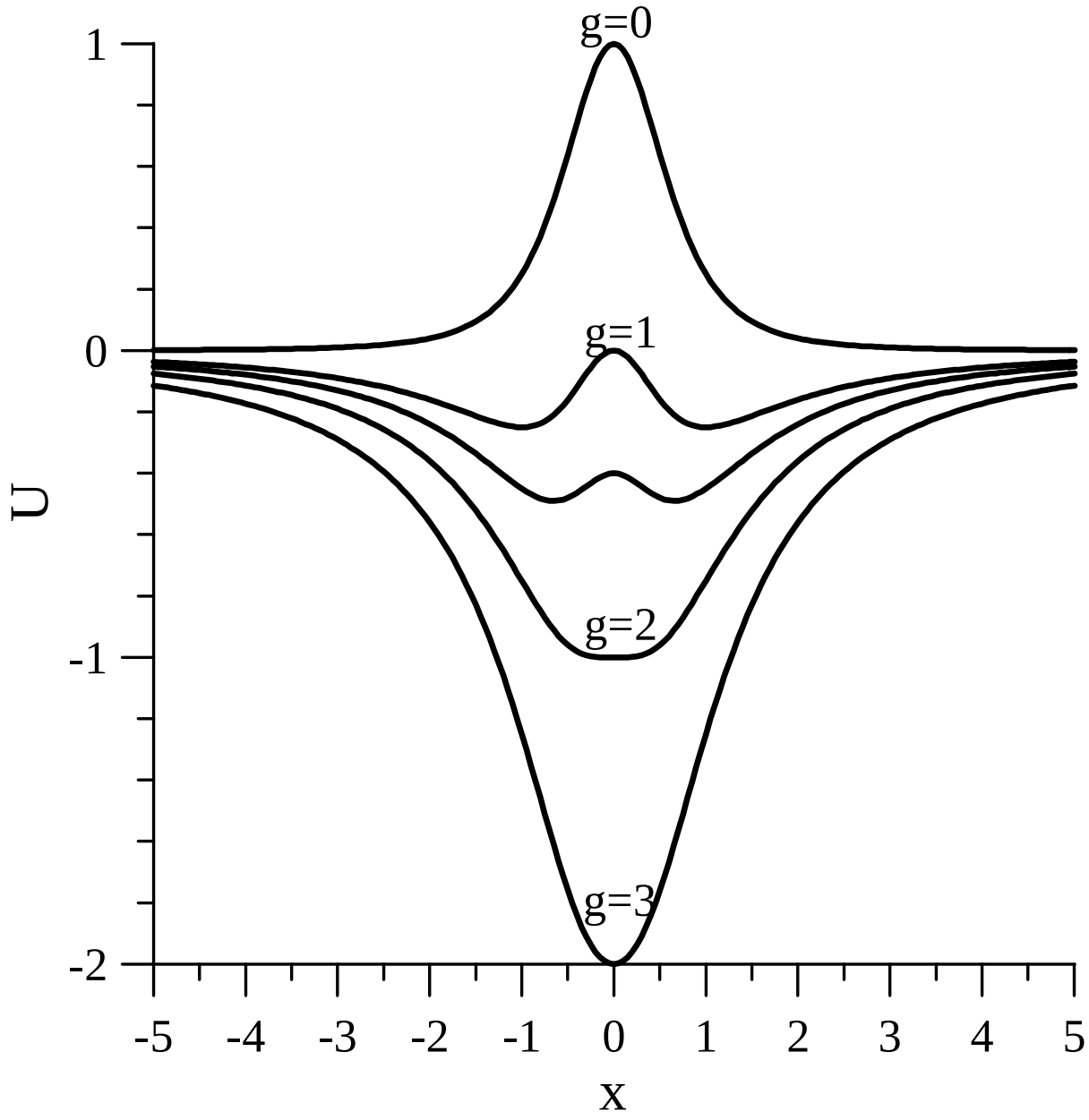

FIG. 1: The potential energy $U(x)$ for various g in the Schrödinger equation (16).

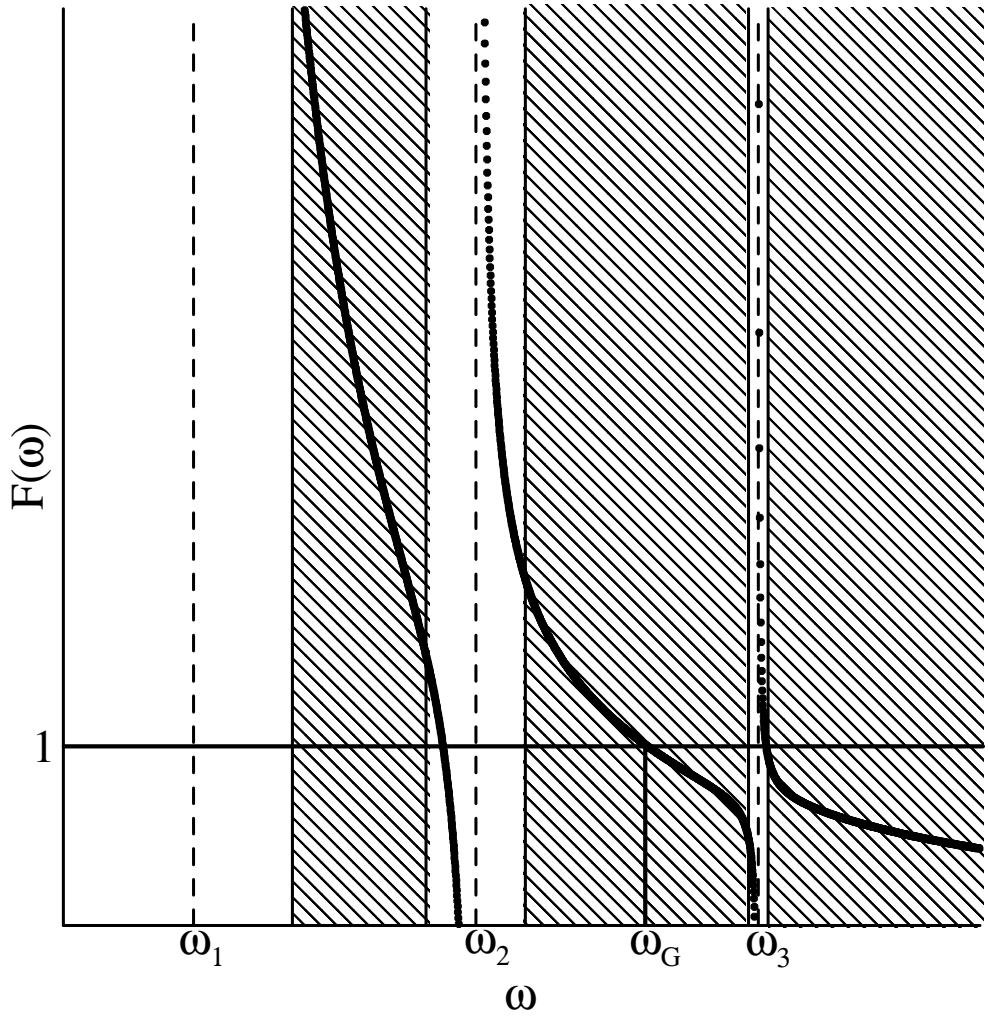

FIG. 2: Sketch of the function $F(\omega)$ given by Eq. (49) with $k_{mn} = 0$ and a possible geodesic acoustic frequency, ω_G. Regions beyond the Alfvén-sound gaps are shaded, the unshaded regions correspond to these gaps, $\omega_\mu = \mu\iota c_s/R$, $\mu = 1, 2, 3$. The frequency ω_G is a continuous function of r only when $\omega_\mu + \Delta_\mu < \omega_G(r) < \omega_{\mu+1} - \Delta_{\mu+1}$ for $0 < r < a$, where Δ_μ is the half-width of the gap; otherwise, $\omega_G(r)$ has jumps at the radii where it crosses the gaps.

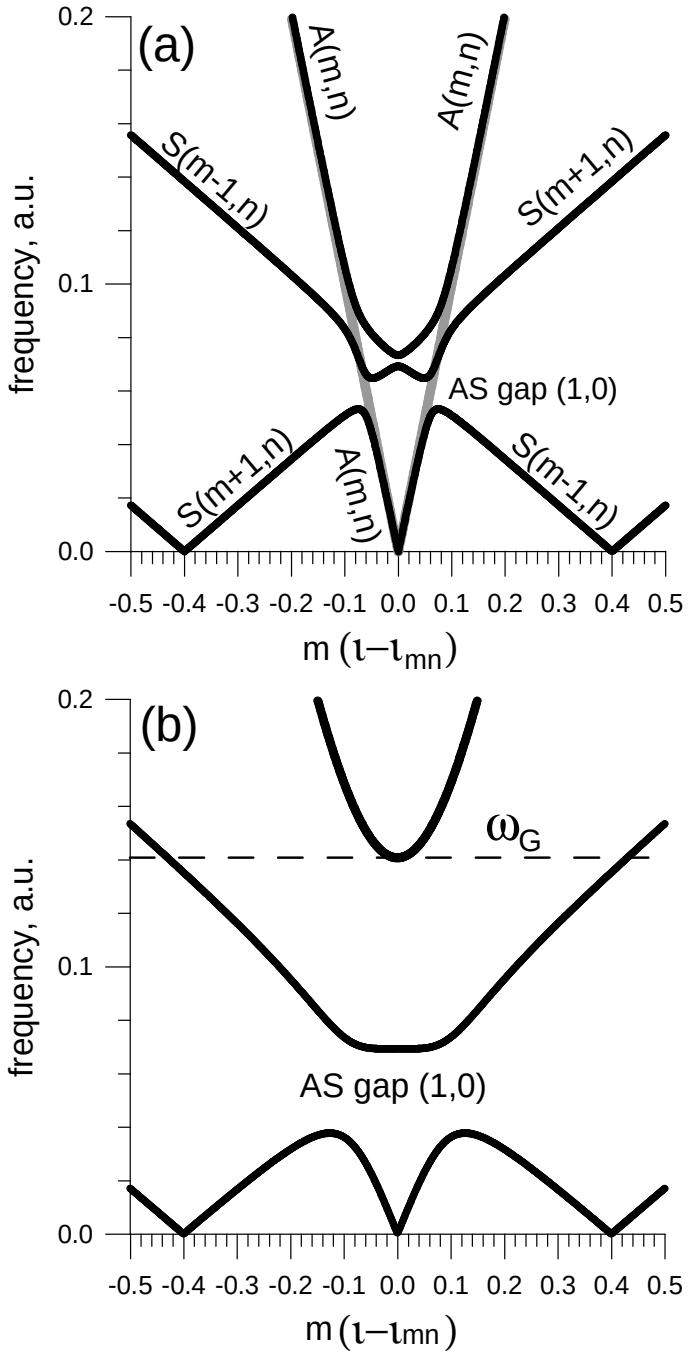

FIG. 3: Sketch of an Alfvén continuum branch, $\omega_{A,mn}$, and sound branches in the vicinity of the rational surface when B_0 has only one (toroidal) harmonic and plasma is homogeneous: (a), $\mathfrak{S} \gg 1$; (b), $\mathfrak{S} \ll 1$. Notations: $\iota_{mn} = n/m$; $A(m,n)$, the Alfvén branch with the mode numbers (m,n); $S(m\pm1,n)$, the sound branches with the mode numbers $(m\pm1,n)$; AS gap $(1,0)$, the Alfvén-sound gap caused by the toroidicity; gray line, the same Alfvén branch in the absence of the Alfvén-sound coupling. We observe that the geodesic acoustic frequency is absent in when $\mathfrak{S} \gg 1$.

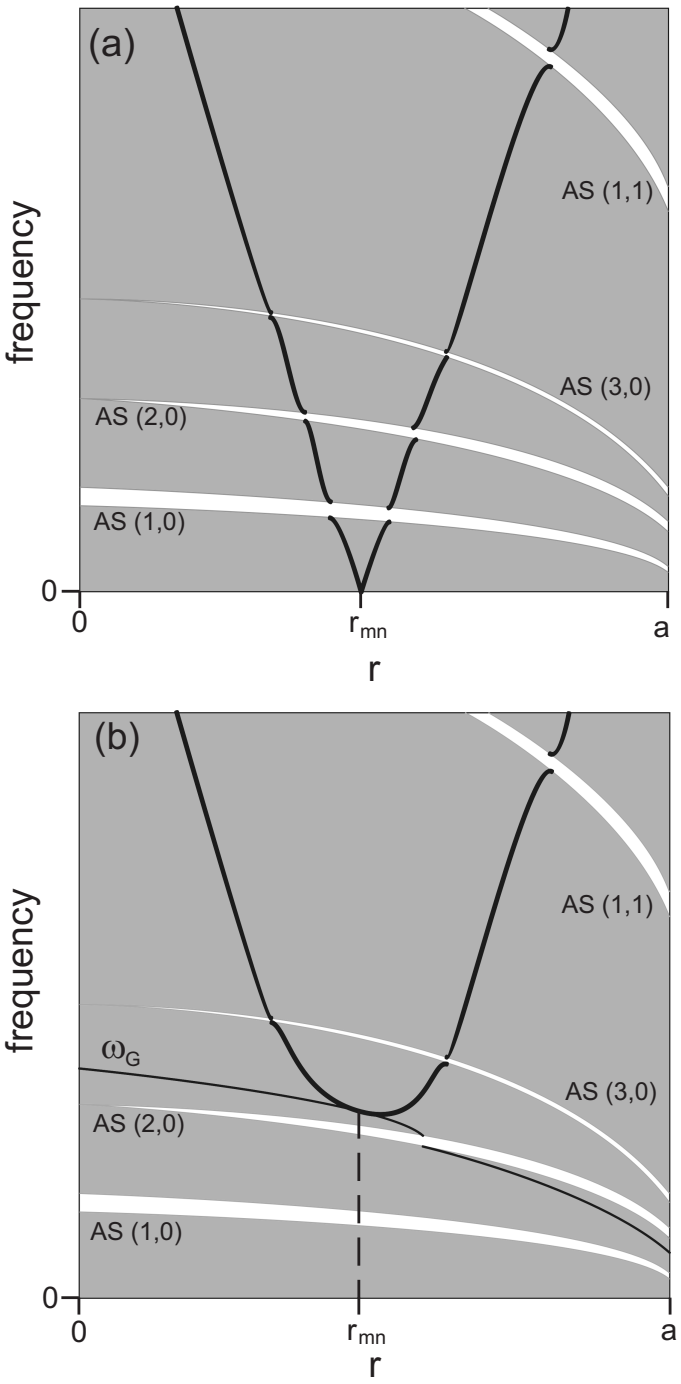

FIG. 4: Sketch of an Alfvén continuum branch for a realistic Fourier spectrum of B_0 and monotonically decreasing plasma temperature: (a) $\mathfrak{S} \gg 1$ (W7-X case); (b) $\mathfrak{S} \ll 1$ (W7-AS case). Notations: gray, continuum (Alfvén and sound) region, white, Alfvén-sound gaps, r_{mn} is the ι_{mn} radius; AS(μ, ν), with μ, ν the integers, are the Alfvén-sound gaps caused by the Fourier harmonics $\epsilon_B^{(\mu\nu)}$. Details of the Alfvén branch in the vicinities of the sound branches are not shown.

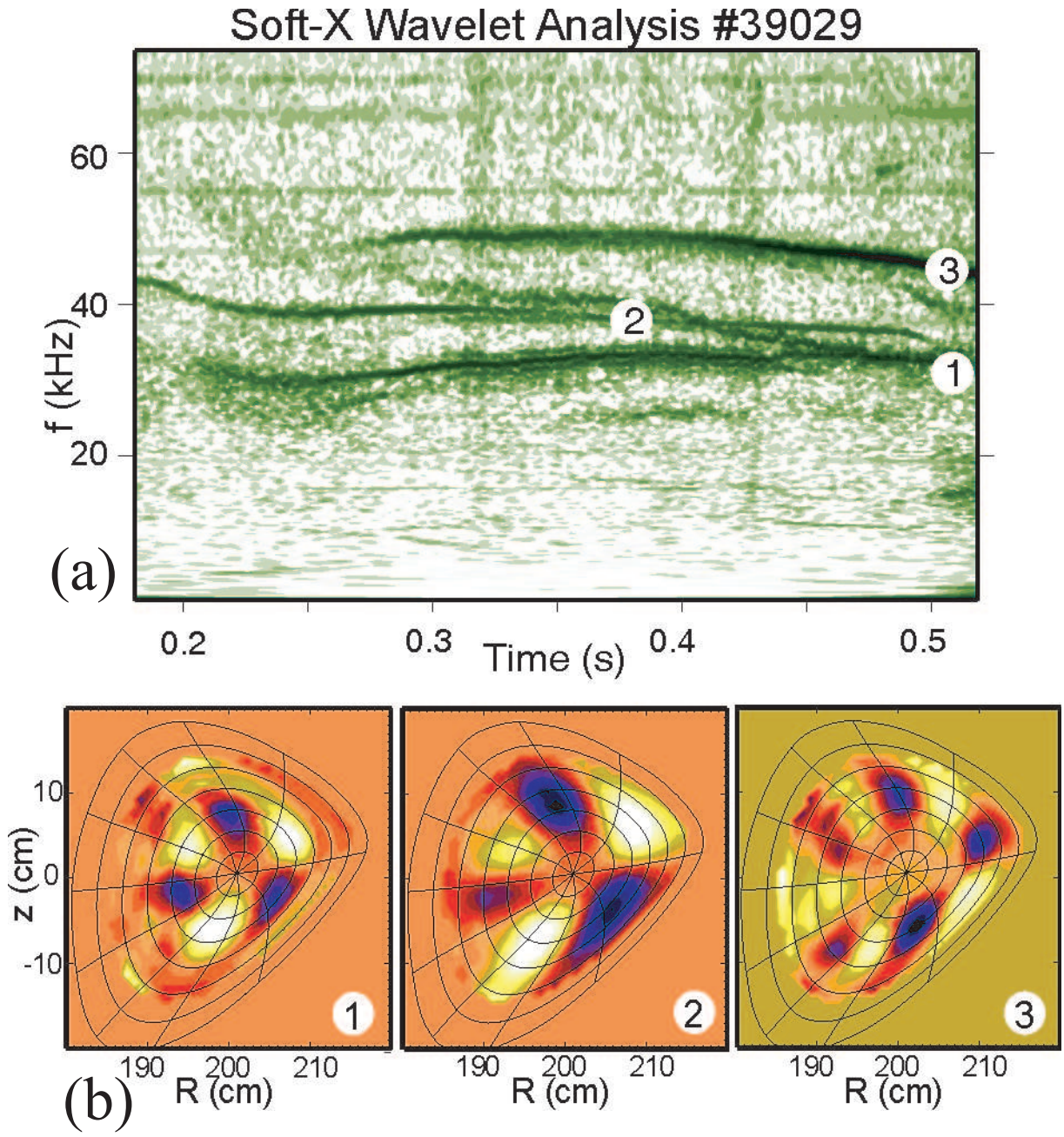

FIG. 5: Alfvénic activity in W7-AS discharge #39029: (a), the frequencies of the $m = 3$ mode in the range of $30 - 40$ kHz and the $m = 5$ mode at $43 - 50$ kHz; (b), the spatial structure of the modes, the mode with the minimum frequency being on the left.

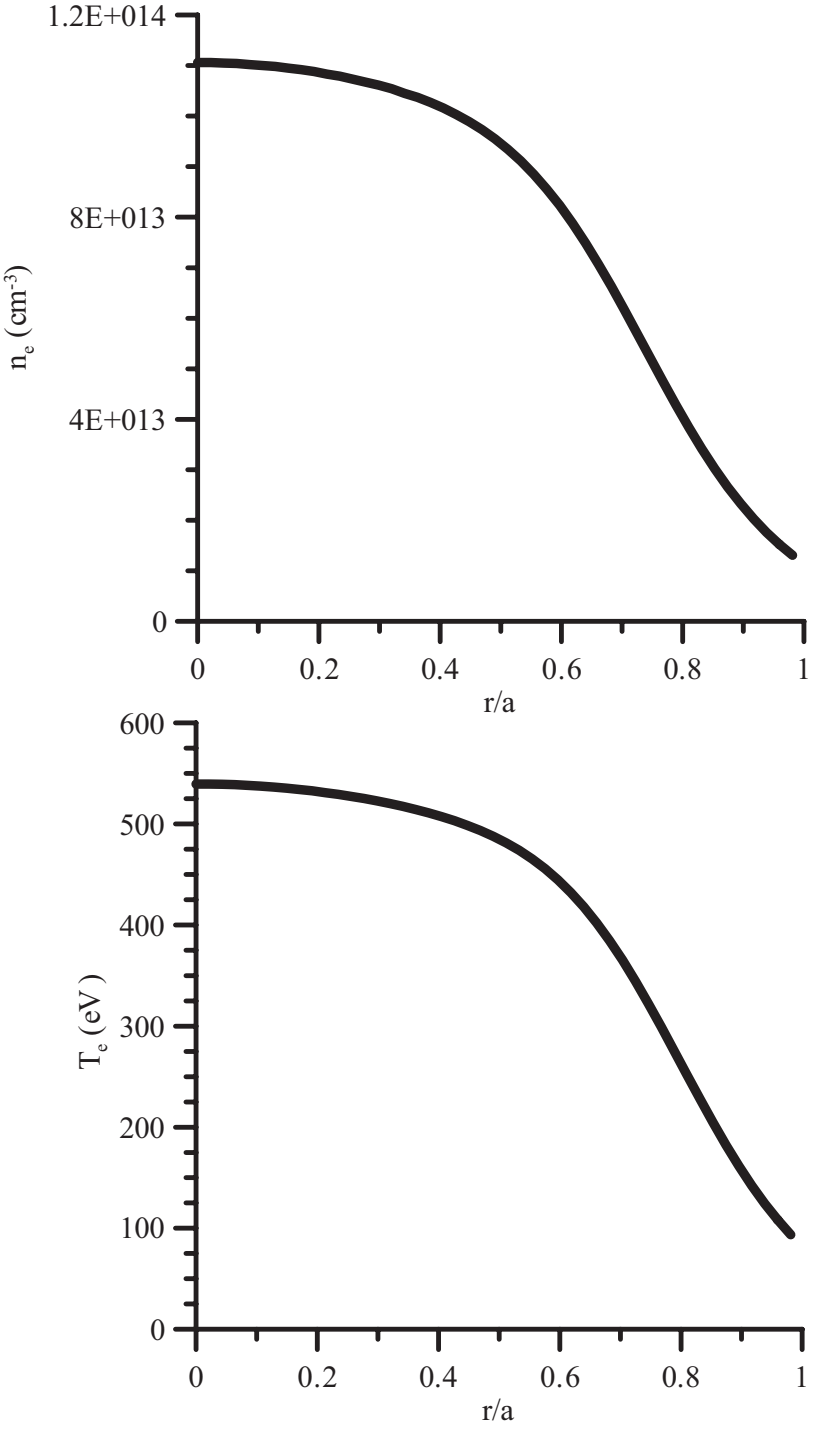

FIG. 6: Radial profiles of the electron density and the electron temperature at $t = 0.45$ s in the W7-AS discharge #39029.

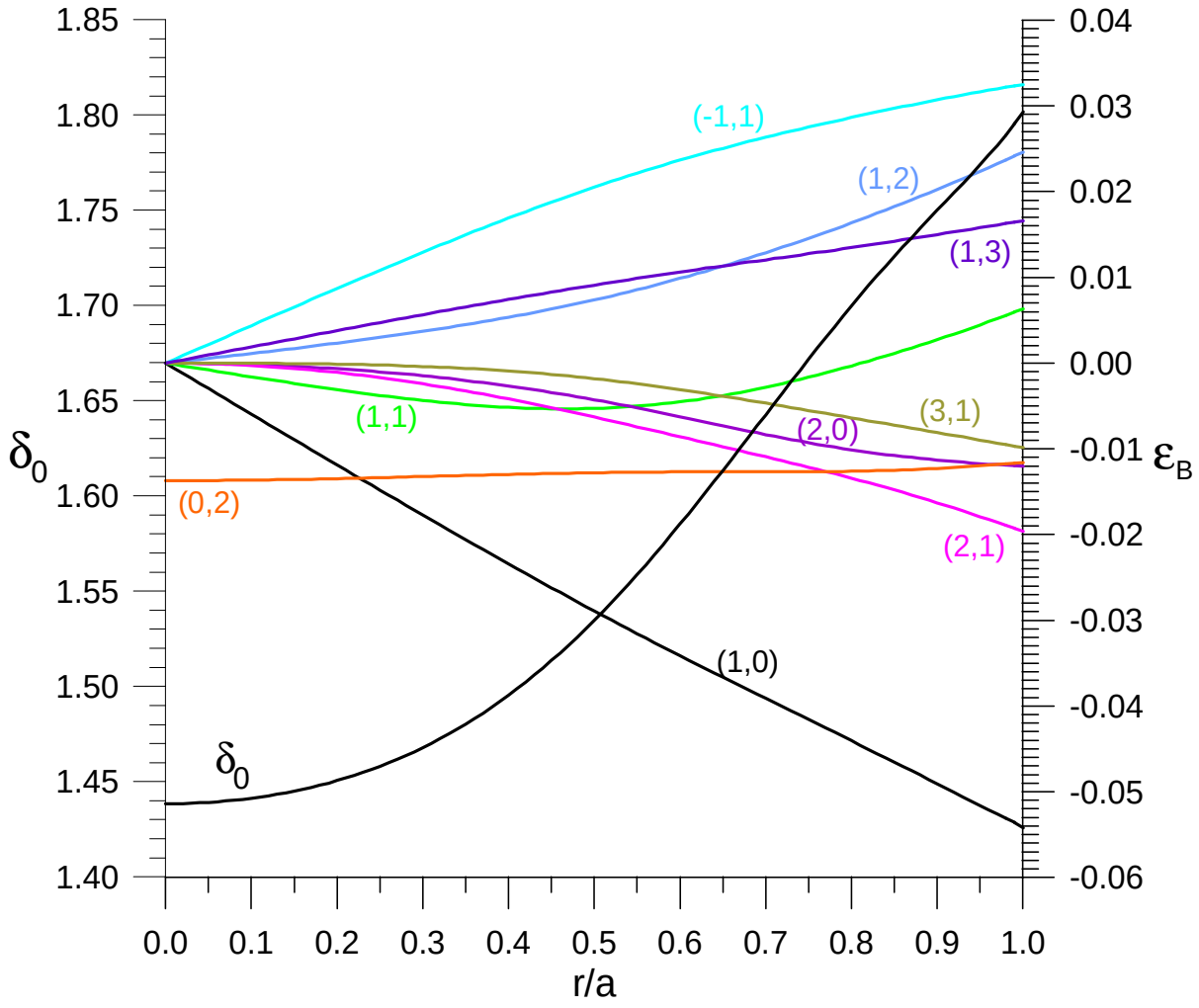

FIG. 7: Fourier harmonics of the equilibrium magnetic field and $\delta_0(r)$ at $t = 0.45$ s in the W7-AS discharge #39029.

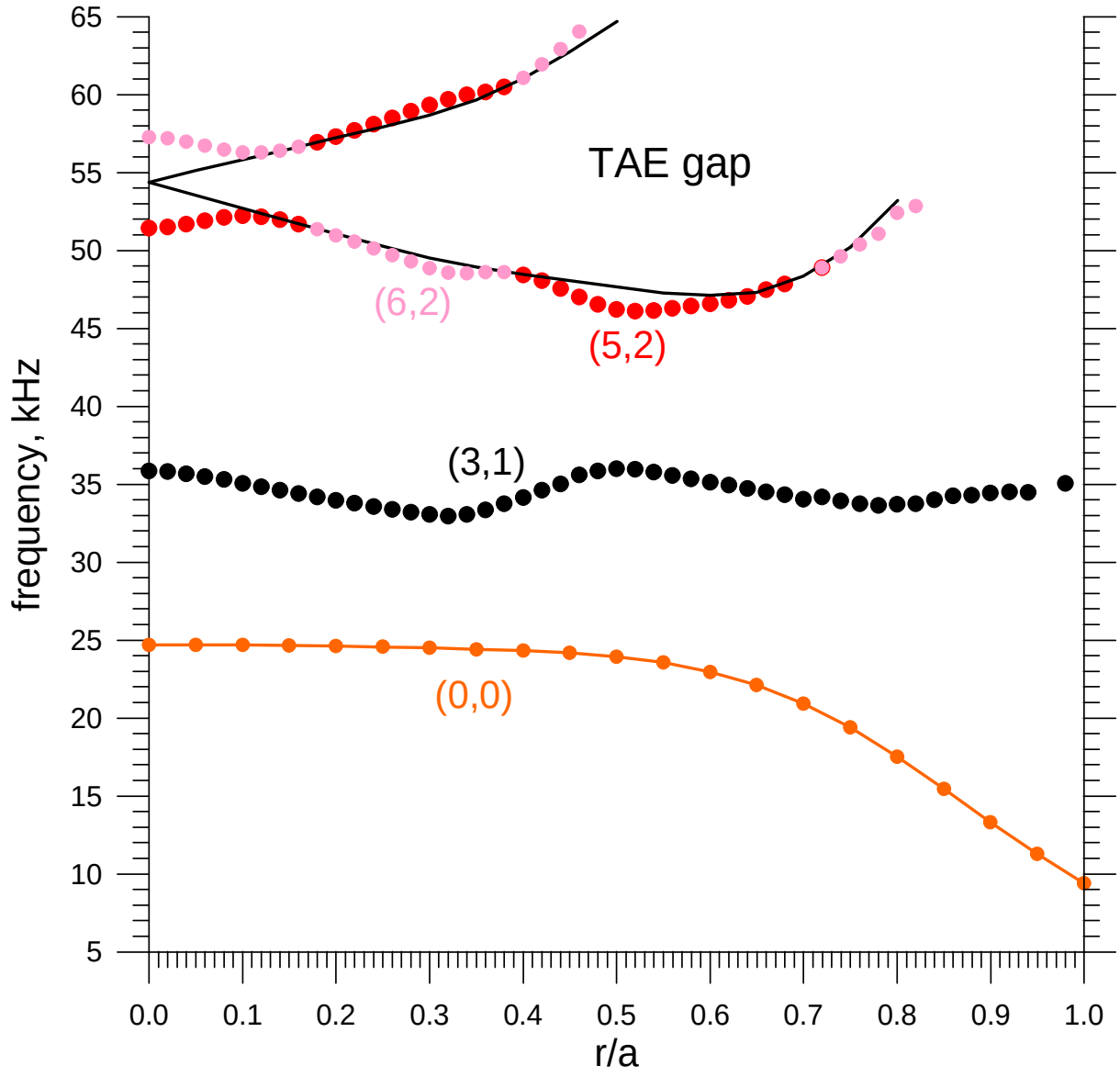

FIG. 8: The Alfvén continuum branches with $m/n = 3/1$ and $m/n = 5/2$ in the W7-AS discharge #39029. The branch with $m/n = 0/0$ represents the geodesic acoustic frequency, ω_G. The calculations were carried out by the code COBRAS.

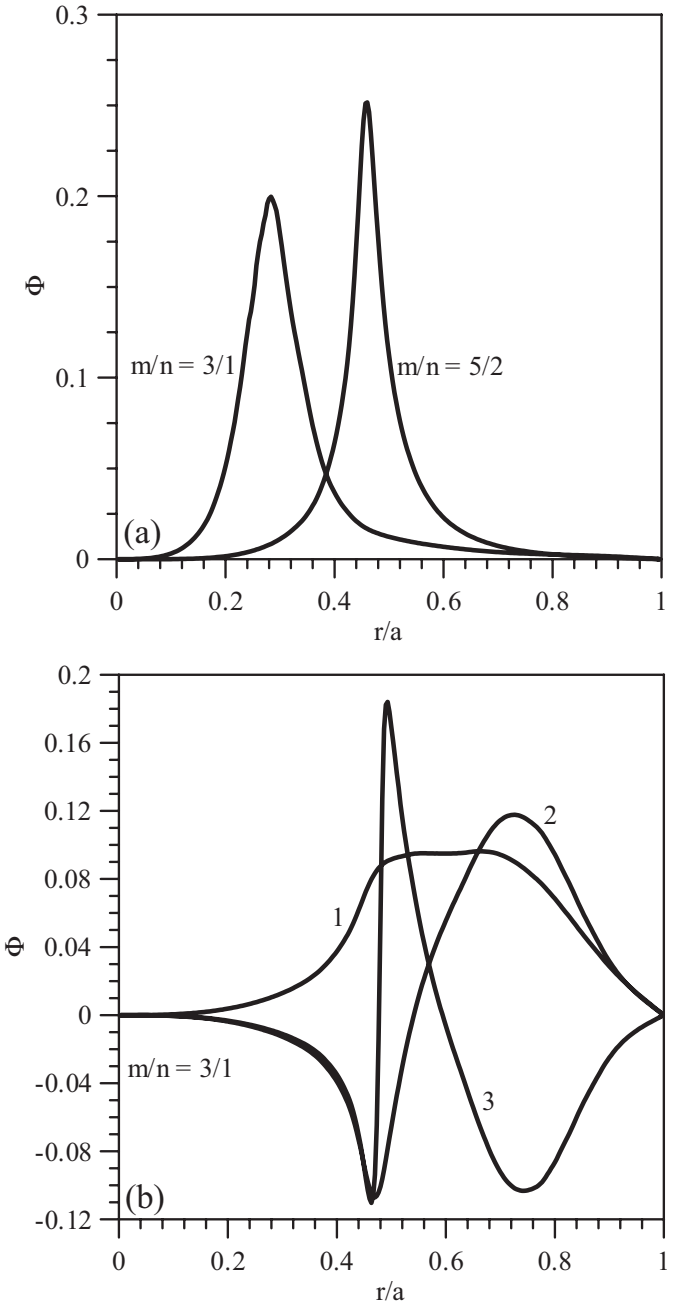

FIG. 9: Alfvén eigenmodes in the W7-AS discharge #39029: (a), $m/n = 3/1$ and $m/n = 5/2$ GAE modes, which are relevant to instabilities with the lowest frequency (33 kHz) and the highest frequency (46 kHz), respectively, shown in Fig. 5 at $t = 0.45$ s; (b), $m/n = 3/1$ NGAE modes relevant to instabilities with intermediate frequencies shown in Fig. 5 at $t = 0.45$ s. Curve 1 is relevant to the instability with the frequency of 38 kHz; curve 3, of 35 kHz. Calculations were carried out by the code BOA-fe.

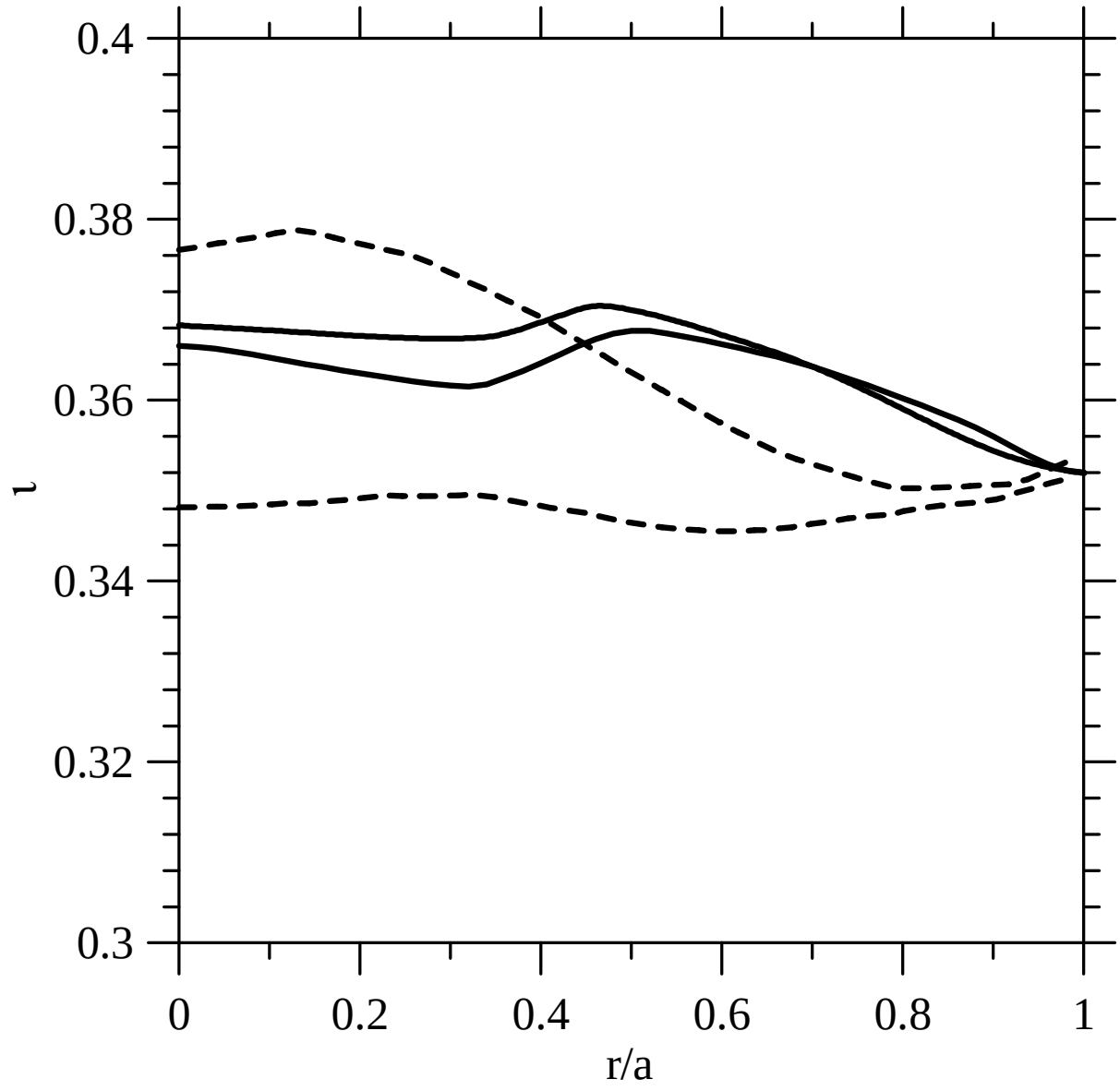

FIG. 10: The rotational transform in W7-AS discharge #39029 at $t = 0.45$ s: upper solid line, reconstructed by using the code BOA-fe; lower solid line, reconstructed by using the code COBRAS; upper dashed line, calculated by the code VMEC with neglecting the NBI-driven current, the bootstrap current, and the OH current; lower dashed line, obtained from the upper dashed line by adding the estimated effect of the bootstrap current and the OH current. Adding the NBI-driven current would increase $\iota(r)$ and might provide a better agreement with the results shown by the solid lines.